



Iron isotopes in an Archean ocean analogue

Vincent Busigny^{a,*}, Noah J. Planavsky^{b,c,*}, Didier Jézéquel^a, Sean Crowe^{d,e},
Pascale Louvat^a, Julien Moureau^a, Eric Viollier^a, Timothy W. Lyons^b^a Institut de Physique du Globe de Paris, Sorbonne Paris Cité, Univ. Paris Diderot, Paris, France^b University of California, Riverside, Department of Earth Sciences, Riverside, CA, USA^c Yale University, Department of Geology and Geophysics, New Haven CT, USA^d University of British Columbia, Department of Microbiology & Immunology, Vancouver, BC, Canada^e University of British Columbia, Department of Earth, Ocean & Atmospheric Sciences, Vancouver, BC, Canada

Received 26 September 2013; accepted in revised form 4 March 2014; Available online 14 March 2014

Abstract

Iron isotopes have been extensively used to trace the history of microbial metabolisms and the redox evolution of the oceans. Archean sedimentary rocks display greater variability in iron isotope ratios and more markedly negative values than those deposited in the Proterozoic and Phanerozoic. This increased variability has been linked to changes in either water column iron cycling or the extent of benthic microbial iron reduction through time. We tested these contrasting scenarios through a detailed study of anoxic and ferruginous Lac Pavin (France), which can serve as a modern analogue of the Archean ocean. A depth-profile in the water column of Lac Pavin shows a remarkable increase in dissolved Fe concentration (0.1–1200 μM) and $\delta^{56}\text{Fe}$ values (-2.14‰ to $+0.31\text{‰}$) across the oxic–anoxic boundary to the lake bottom. The largest Fe isotope variability is found at the redox boundary and is related to partial oxidation of dissolved ferrous iron, leaving the residual Fe enriched in light isotopes. The analysis of four sediment cores collected along a lateral profile (one in the oxic layer, one at the redox boundary, one in the anoxic zone, and one at the bottom of the lake) indicates that bulk sediments, porewaters, and reactive Fe mostly have $\delta^{56}\text{Fe}$ values near $0.0 \pm 0.2\text{‰}$, similar to detrital iron. In contrast, pyrite $\delta^{56}\text{Fe}$ values in sub-chemocline cores (60, 65, and 92 m) are highly variable and show significant deviations from the detrital iron isotope composition ($\delta^{56}\text{Fe}_{\text{pyrite}}$ between -1.51‰ and $+0.09\text{‰}$; average -0.93‰). Importantly, the pyrite $\delta^{56}\text{Fe}$ values mirror the $\delta^{56}\text{Fe}$ of dissolved iron at the redox boundary—where near quantitative sulfate and sulfide drawdown occurs—suggesting limited iron isotope fractionation during iron sulfide formation. This finding has important implications for the Archean environment. Specifically, this work suggests that in a ferruginous system, most of the Fe isotope variability observed in sedimentary pyrites can be tied to water column cycling—foremost to the oxidation of dissolved ferrous iron. This supports previous suggestions that enhanced iron isotope variability in the Archean may record a unique stage in Earth's history where partial ferrous iron oxidation in upwelling water masses was a common process, probably linked to oxygenic or anoxygenic photosynthesis.

© 2014 Elsevier Ltd. All rights reserved.

1. INTRODUCTION

Changes in the iron cycle through time have played a key role in shaping global biogeochemical evolution (Johnson et al., 2008b; Poulton and Canfield, 2011). Iron isotopes have emerged in the past decade as tracers of iron cycling on the early Earth—paving the way to test long-standing

* Corresponding and equal contribution authors. Tel.: +33 1 83 95 74 34 (V. Busigny). Addresses: Yale University, Department of Geology and Geophysics, New Haven CT, USA (N.J. Planavsky), Institut de Physique du Globe de Paris, Sorbonne Paris Cité, Univ. Paris Diderot, Paris, France (V. Busigny).

E-mail addresses: busigny@ipgp.fr (V. Busigny), noah.planavsky@yale.edu (N.J. Planavsky).

models about the chemical evolution of the ocean (Dauphas and Rouxel, 2006; Anbar and Rouxel, 2007; Johnson et al., 2008b). There are several well-established trends in the global sedimentary iron isotope record across geologic time (Fig. 1). These trends are most prevalent in the pyrite record but are also observed from bulk-rock analyses of organic-rich shales and carbonates (e.g., Rouxel et al., 2005; Johnson et al., 2008b). Archean and Paleoproterozoic pyrites, studied by analysis of isolated pyrite crystals or chemical sequential extraction, have $\delta^{56}\text{Fe}$ values that range from -3.51 to $+1.19$ per mil (‰), while modern, Phanerozoic, and Neoproterozoic sedimentary pyrites show a much narrower range in $\delta^{56}\text{Fe}$ values between -1.65 ‰ and $+0.16$ ‰ (Rouxel et al., 2005; Fehr et al., 2010). Throughout Earth's history, a larger range of $\delta^{56}\text{Fe}$ values is recorded in ancient sediments probed by microanalysis techniques (secondary ion mass spectrometry or laser ablation systems; Steinhofel et al., 2009, 2010; Yoshiya et al., 2012; Virtasalo et al., 2013). However, these values likely track both small-scale diagenetic processes and fluctuating water column chemistry and therefore cannot readily be compared to other bulk sedimentary iron isotope records.

The greatest amount of iron isotope variability identified in the sedimentary record (Fig. 1; Rouxel et al., 2005; Johnson et al., 2008a) is found in Neoproterozoic rocks deposited between 2.9 and 2.5 Ga, clearly delineating an enigmatic yet unique period of iron cycling. There are a few possible

explanations for the presence of markedly light $\delta^{56}\text{Fe}$ values in the Archean sedimentary rock record. The highly negative $\delta^{56}\text{Fe}$ values have been proposed to mark the onset of extensive benthic dissimilatory iron reduction (Johnson et al., 2008b; Heimann et al., 2010). In this case, the iron isotopes would record fundamental changes in marine heterotrophic communities through time. Alternatively, the markedly negative $\delta^{56}\text{Fe}$ values and their disappearance from the sedimentary record over time might indicate a shift in the chemical composition of the oceans tied to processes other than microbial iron reduction. Specifically, the negative $\delta^{56}\text{Fe}$ values may instead result from partial oxidation of the dissolved iron pool, producing a dissolved residue depleted in heavy Fe isotopes, which can be transferred to the rock record as pyrite (Rouxel et al., 2005). In this model, the iron isotope composition of marine sediments would track the oxidation of the oceans. Lastly, it has also been proposed that in iron-rich aqueous systems, pyrite will be isotopically light due to large kinetic isotope fractionations (Guilbaud et al., 2011). The sedimentary iron isotope composition will then record marine dissolved iron availability, with markedly negative $\delta^{56}\text{Fe}$ values and greater isotope variability reflecting a large dissolved Fe reservoir, dominating over reduced S compounds (Guilbaud et al., 2011). This model is intriguing in that it requires us to rethink how ocean chemistry has changed through time given that iron-rich marine conditions are now widely envisioned

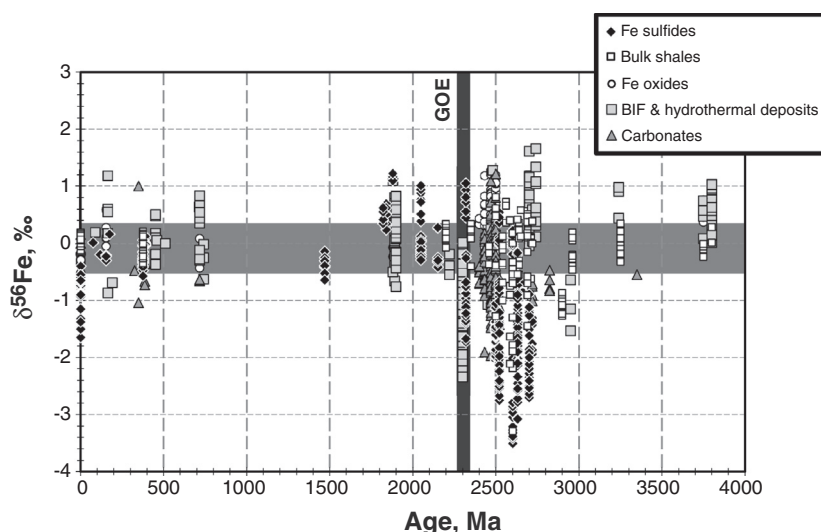


Fig. 1. Iron isotope composition of sedimentary minerals and bulk rocks through time. Data on Fe sulfides, oxides, and carbonates, together with bulk shales, iron formation and hydrothermal deposits are compiled from the literature. For comparison, the horizontal light-grey zone represents the range of Fe isotope compositions for detrital sediments and hydrothermal fluids. Earth's earliest sedimentary record (3.8–3.0 Ga) is characterized by near crustal or positive $\delta^{56}\text{Fe}$ values, suggesting a biosphere with limited oxidative capacity. After 3.0 Ga but prior to the rise of atmospheric oxygen (so called Great Oxidation Event, GOE) at ~ 2.4 Ga, there were sedimentary pyrites and shales with anomalously negative $\delta^{56}\text{Fe}$ values. Data compiled for pyrites, Fe oxides and carbonates are from Johnson et al. (2003, 2008a), Matthews et al. (2004), Rouxel et al. (2005), Archer and Vance (2006), Severmann et al. (2006), Staubwasser et al. (2006), Busigny and Dauphas (2007), Dauphas et al. (2007a, b), von Blanckenburg et al. (2008), Duan et al. (2010), Craddock and Dauphas (2011), Halverson et al. (2011), Czaja et al. (2012). Carbonates from high-grade metamorphic rocks from Greenland and Canada were avoided due to their possible metasomatic origins. Data on bulk shales, banded iron formation and hydrothermal deposits are from Matthews et al. (2004), Yamaguchi et al. (2005), Staubwasser et al. (2006), Severmann et al. (2006), Frost et al. (2007), Dauphas et al. (2007a, b), Valaas Hyslop et al. (2008), Planavsky et al. (2009, 2012), Steinhofel et al. (2009), Tsikos et al. (2010), Duan et al. (2010), Halverson et al. (2011) and Czaja et al. (2012). Iron isotope data obtained using Ion Microprobe and Laser Ablation MC-ICP-MS analyses were discarded from the present compilation because the large heterogeneities observed on small-scale (within single crystals) that are not linked to marine biogeochemical iron cycling.

to have persisted well past the observed time interval of enhanced iron isotope variability (e.g., Planavsky et al., 2011; Poulton and Canfield, 2011). Constraining the origin of negative Archean $\delta^{56}\text{Fe}$ values, therefore, will not only improve our understanding of iron isotope systematics but will also advance our understanding of Earth's biogeochemical evolution.

Debate on the origin of negative $\delta^{56}\text{Fe}$ values stems in part from the lack of work in modern aqueous systems that are analogous to the early oceans. The early oceans are thought to have had low sulfate concentrations (e.g., Habicht et al., 2002) and a significant dissolved iron reservoir (Holland, 1984). These characteristics may be essential in allowing for enhanced iron isotope fractionations during microbial iron reduction (Johnson et al., 2008b) or during inorganic pyrite precipitation (Guilbaud et al., 2011). In stark contrast to the increasing number of studies on sulfide-rich, iron-poor modern anoxic basins (e.g. Fehr et al., 2008, 2010; Severmann et al., 2008; Staubwasser et al., 2013), there has been limited work on low sulfate, iron-rich modern aqueous systems to test these models (Malinovsky et al., 2005; Teutsch et al., 2009; Song et al., 2011). With this in mind, we have conducted a detailed iron isotope study in ferruginous Lac Pavin in the French Massif Central, an aquatic system that may serve as one of our best modern analogs for the Earth's early ferruginous oceans.

Lac Pavin is permanently redox-stratified, with anoxic and ferruginous deep waters (from 60 to 92 m depth) topped by oxic shallow waters (from 0 to 60 m). It contains dissolved ferrous Fe (up to 1.2 mM) below the chemocline at ~60 meters (Michard et al., 1994; Viollier et al., 1995). Additionally, the lake has remarkably low sulfate concentrations (<20 μM). Lac Pavin, therefore, has conditions similar to those inferred for Archean oceans—that is, high dissolved Fe concentrations, a strong vertical gradient in dissolved iron concentrations, and low levels of sulfate and sulfide (e.g., Sumner, 1997; Beukes and Gutzmer, 2008).

In the present work, we analyzed Fe concentrations and isotope compositions along a depth-profile in the water column of Lac Pavin. To track the record of water column Fe cycling and its isotopic effect, we also collected four sediment cores: one from the oxic zone (32 m), two from below but near the chemocline under anoxic waters (60, 65 m), and one from the anoxic bottom of the lake (92 m). Following Severmann et al. (2006), we determined iron isotope compositions for the bulk, reactive (labile Fe phases such as amorphous Fe-oxides, FeS, and potentially some reactive silicate Fe), pyrite, and porewater iron in each of the cores. Based on dissolved Fe data from the water column with solid phase and porewater analyses from sediment cores, we suggest that benthic iron recycling and kinetic isotope fractionations during pyrite formation have little to no effect on the sedimentary iron isotope record. Instead, our iron isotope work in Lac Pavin provides evidence for iron oxidation in the water column controlling the iron isotope composition of underlying sediments in the lake and likely in many ancient systems, by analogy.

2. SAMPLES AND METHODS

2.1. Overview of Lac Pavin

Lac Pavin is a crater lake, within the youngest volcano in the French Massif Central. The last volcanic eruption and the ensuing lake formation occurred ~6900 years ago (Juvigné and Gilot, 1986; Chapron et al., 2010). It is located 35 km southwest of Clermont-Ferrand, 1197 m above sea level (45°29.740N, 2°53.280E). The lake is a maar, i.e., a crater lake resulting from a phreatomagmatic eruption (Glangeaud, 1916). It is characterized by a high aspect ratio (maximum depth/surface^{0.5} = 0.138), a surface area of ~0.445 km², a diameter of ~750 m, and a maximum depth of ~92 m. Because of this specific lake geometry and wind protection afforded by the surrounding tuff-ring (~50 m high), water column mixing is depth-limited. Lac Pavin is meromictic with two stable stratified layers (Fig. 2a). The three factors common to most meromictic settings are present in this lake: appreciable biological production in the surface waters, ectogenic controls, and crenogenic inputs (deep water inflow via springs) (Assayag et al., 2008; Bonhomme et al., 2011). The upper layer, called mixolimnion, extends from the surface to ca. 60 m depth and is oxygenated because of seasonal mixing. The deeper layer, called monimolimnion, extends from 70 to 92 m depth and never mixes with upper oxygenated waters. The monimolimnion is oxygen depleted due to high organic matter load, and has been permanently anoxic over the last 100 years, at least (Glangeaud, 1916). An intermediate layer, called mesolimnion, which is characterized by sharp dissolved Fe and salinity gradients, separates the mixolimnion and monimolimnion. Over the last 40 years, the physicochemical conditions of the lake and associated sediments have been studied extensively, and geochemical cycling of many elements is well constrained (for example, C, Fe, P, N, and S). On a decadal time scale, the available data show that the deep part of the lake (below 60 m depth) has reached a steady state (Michard et al., 1994, 2003; Aeschbach-Hertig et al., 1999; Jézéquel et al., 2011). It is thus an ideal natural laboratory to study Fe cycling and associated isotope fractionations in a stratified water body.

The chemical profiles in the mixolimnion are shaped by the activity of photosynthetic organisms and associated heterotrophs. Oxygen (O₂) is produced by photosynthesis and accumulates in the photic zone (Assayag et al., 2008), while nutrients such as nitrate (NO₃⁻) and phosphate (PO₄³⁻) are depleted due to biological assimilation (Fig. 2; Michard et al., 1994). Diatoms make up the majority of the planktonic biomass in the photic zone (Amblard and Bourdier, 1990) and draw down dissolved silica levels within the mixolimnion. Dissolved Fe and sulfate (SO₄²⁻) concentrations in the mixolimnion are a few tens of nM and 15–20 μM , respectively (Fig. 2; Michard et al., 1994, 2003).

The monimolimnion is devoid of oxygen but contains very high concentrations of dissolved ionic species, as shown by the strong increase in specific conductivity with depth (Fig. 2b). These high concentrations induce high-density anoxic deep water that counter balances the ~1 °C temperature increase observed below 60 m depth

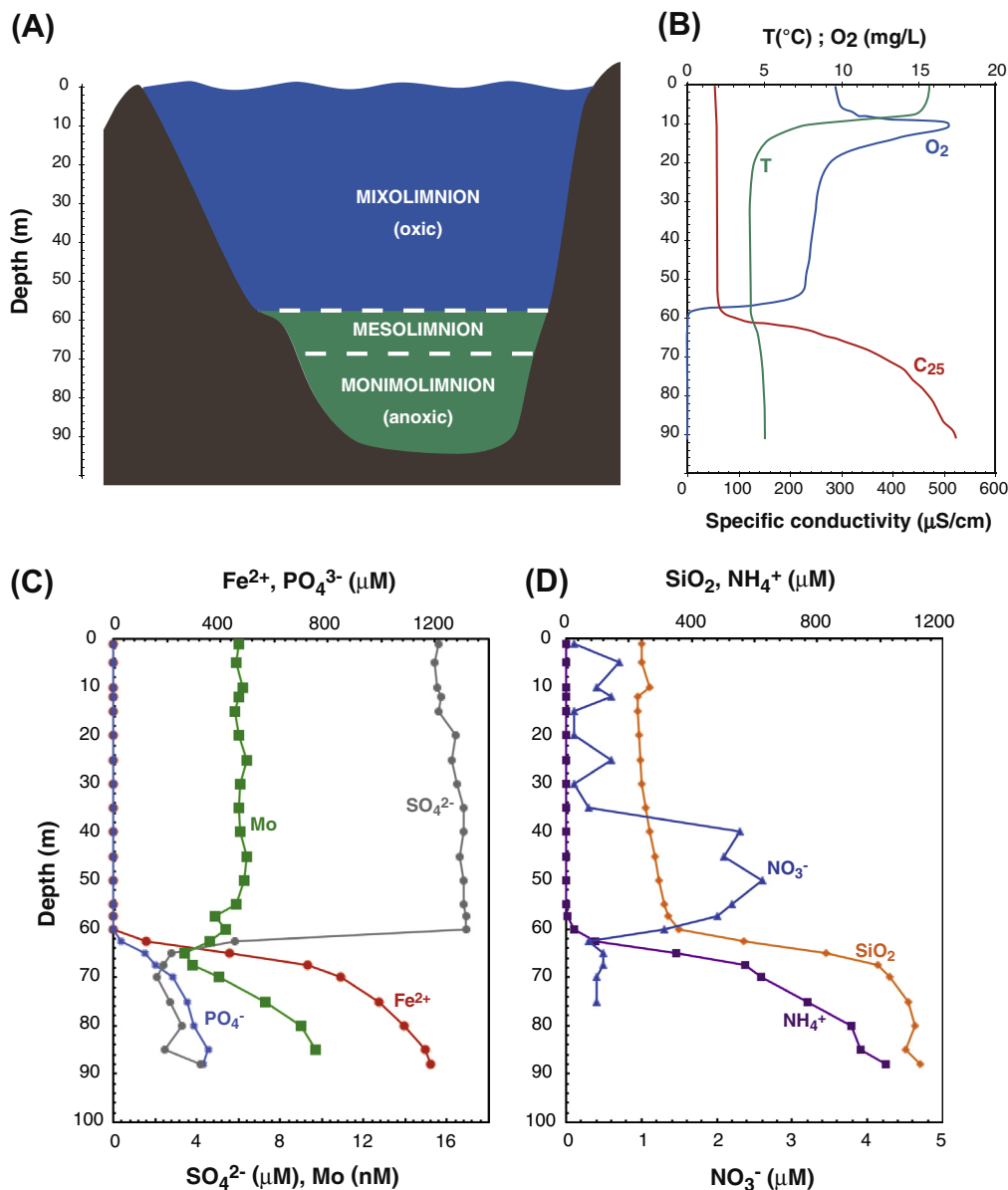


Fig. 2. Illustration of the physico-chemical stratification in Lac Pavin. (A) Schematic profile of the Lake. (B) Temperature, dissolved oxygen content and specific conductivity (expressed as C₂₅) determined in July 2007. (C) and (D) Selected dissolved chemical species (data from Michard et al., 1994; Viollier et al., 2000).

and thus contributes to maintaining water column stratification. The main charged dissolved species in the monimolimnion are bicarbonate (HCO_3^-), ferrous iron (Fe^{2+}), ammonium (NH_4^+) (with concentrations of up to 4.8, 1.1, and 1 mM, respectively). The main uncharged species are carbonic acid (H_2CO_3), methane (CH_4), and dissolved silica (H_4SiO_4) (with concentrations of up to 12.1, 4.3 and 1.1 mM, respectively) (Fig. 2; Michard et al., 1994). Phosphate is also highly concentrated and reaches up to 340 μM . Accumulation of the reduced compounds as well as carbonate species mainly derives from sub-mixolimnion organic matter remineralization. Sulfate is reduced to sulfide just below the oxycline (>60 m) with sulfate drawdown to stable low μM levels (Bura-Nakic et al., 2009).

Most major compounds and nearly all measured trace elements show strong concentration gradients, with high concentrations at the sediment–water interface and low concentrations at the oxycline (Michard et al., 1994, 2003; Viollier et al., 1995; Takayanagi and Cossa, 1997). These concentration gradients reflect upward diffusion of dissolved ions sourced from the sediment and consumed at the redox boundary. This is the case for iron, which is released from the sediment in the ferrous form (Fe^{2+}) and precipitates as ferric iron (Fe^{3+}) at the redox interface (Michard et al., 2003). Because of high stability, the monimolimnion is enriched in dissolved gases such as CH_4 produced by microbial methanogenesis (Biderre-Petit et al., 2011) and CO_2 resulting from anaerobic respiration,

anaerobic CH₄ oxidation, and/or a deep spring input related to volcanic activity (Aeschbach-Hertig et al., 1999; Olive and Boulègue, 2004; Assayag et al., 2008; Lopes et al., 2011). Microbial density (bacteria and archaea) increases with depth from 50 m to the bottom of the lake (Lehours et al., 2007)—following the increase in dissolved ion species. Facultative Fe(III) reducing bacteria are likely present, but well-known obligatory Fe(III) reducers (such as *Geobacter*) have not been identified (e.g., Lehours et al., 2009).

The sediments deposited in Lac Pavin are dominated by diatom silica frustules, organic matter, authigenic iron minerals, and detrital components (Meybeck et al., 1975; Schettler et al., 2007; Cosmidis et al., 2014). SiO₂ content generally varies between 20 and 70 wt%, and bulk organic carbon between 4 and 18 wt%. The Fe_{Bulk} concentrations in bottom sediments are elevated (2.5–25 wt%) compare to Al (2–7 wt%)—with Fe/Al molar ratios of 0.3–36 (Schettler et al., 2007), which are either similar to or well above the crustal average and the ratio observed for volcanic rocks in the Pavin catchment (see discussion below). Extreme iron-enrichment found in Lac Pavin sediments is similar to deposits of the Earth's early oceans. This relationship indicates that a large portion of Fe is authigenic and precipitates in the water column and/or from sediment porewaters. Authigenic Fe phases in Lac Pavin sediments are mostly siderite (ferrous carbonate) and vivianite (ferrous phosphate), together with iron sulfide (iron monosulfides, and pyrite) (Viollier et al., 1997; Schettler et al., 2007; Cosmidis et al., 2014). A detailed mineralogical study demonstrated that ferric particles were present in the water column but could not be found in the lake bottom sediment, suggesting intense Fe reduction at the sediment water interface (Cosmidis et al., 2014). These ferric particles were mainly Fe oxyhydroxides in both oxic and anoxic waters, and some ferric phosphates, which were found only in anoxic waters, at and below the chemocline.

2.2. Sample collection and description

Four sampling campaigns were carried out from 2006 to 2009. The goal of the first one in November 2006 was to test if Fe isotopes were fractionated during sample collection, with particular attention paid to filtration processes on board under atmospheric conditions (see results in Appendix A). The second campaign, conducted in July 2007, focused on the collection of water samples along a vertical profile in the water column from 55 to 90.5 m depth, and constraining sulfur cycling in the mesolimnion and monimolimnion (Bura-Nakic et al., 2009). Dissolved oxygen, temperature, and specific conductivity were determined using a Seabird SBE 19 Seacat profiler (Sea-Bird Electronics Inc., Washington, DC; Fig. 2b). During the third campaign in July 2009, we collected three sediment cores from different depths: 32 m (oxic zone; 45°29.912N, 2°53.257E), 60 m (redox interface; 45°29.833N, 2°53.267E), and 65 m (anoxic zone; 45°29.822N, 2°53.207E). These cores were taken using a Mortimer gravity corer, allowing us to sample a vertical profile over 10–14 cm below the water–sediment interface. During the fourth and last sampling campaign in September 2009, a sediment core from the deepest part of

the lake (~92 m; 45°29.743N, 2°53.279E) was collected using an Uwitec gravity corer with a diameter of 90 mm. The total length recovered from this core was 167 cm. In the present study, we focused only on the first half of this core, from the top down to 83.5 cm.

Water samples were collected from a sampling platform anchored near the center of the lake (45°29.745N, 2°53.274E) using an 1-L syringe sampler. The sampler was a custom-built automatic polycarbonate syringe (modified from the Model S-1000, Hamilton®), equipped with an electronic depth gauge allowing a precision of ±0.2 m depth. Waters were filtered to 0.2 μm using Millipore cellulose acetate membranes and were then acidified with a few drops of ultrapure HNO₃ to pH 1–2. All samples were stored at 4 °C until chemical and isotope analyses were conducted.

Sediment cores were transferred into glove bags and placed under anoxic conditions (N₂ pressure) immediately after collection. They were processed and split into cm-scale fractions along the core's vertical axis. The porewaters were separated from the solid phases once extracted from the core barrel using Rhizon® samplers connected via tubing to septum capped vials under vacuum (filtration to 0.2 μm) and were then acidified with ultrapure HCl. During the whole separation process, oxygen levels were monitored with an Oxi 340i WTW oxygen meter and were always below the detection limit of 0.1 mg/L. The solid phases were then frozen, and the porewaters were stored at 4 °C. The solid phase of the 90 m core was fully dehydrated by freeze drying before analysis.

Three volcanic rocks were collected from outcrops of the inner Pavin crater and are assumed to represent the detrital Fe flux to the lake sediments. These volcanics are trachybasalts formed by eruption of the Puy de Montchal, a volcano overhanging the Pavin crater on its south side. Texturally, samples RUD#1 and RUD#2 are vesicle-rich trachybasalts, while RUD#3 is massive and mostly vesicle-free. Thin section observations and electron microprobe analyses indicate that these three samples are composed of olivine, clinopyroxene (augite), and plagioclase feldspar microliths in a glass matrix, with minor titanomagnetite. The sample RUD#1 also contained additional hornblende. Limited secondary phases, such as Fe oxyhydroxides and clay minerals formed by partial alteration of the rocks, were also observed in the thin sections. Electron microprobe analyses for all three samples show Fe/Al molar ratios of ~0.3 for the glasses and ~0.1 for clay minerals. In order to evaluate if alteration processes of the trachybasalts could produce Fe isotope fractionation and thus modify the isotope signature of the detrital Fe flux, the three samples were cut into several sub-samples. RUD#1 and RUD#2 were split into two sub-samples: (1) a “dark” core lacking any visible surface alteration (RUD#1-C and RUD#2-C) and (2) a “lighter” border apparently affected by alteration (RUD#1-B and RUD#2-B). Sample RUD#3 was characterized by a clear light-grey alteration rind on its outer rim and was divided into a core (RUD#3-C), alteration rind (RUD#3-A), and an intermediate sub-sample between the core and the outer altered rind (RUD#3-M).

2.3. Chemical analyses: Fe(II)/Fe(III), Mn(II), and SO_4^{2-} concentrations

The dissolved Fe(II)/Fe(III) speciation was performed on board using filtered samples from the water column and spectrophotometric measurement (Merck SQ300 spectrophotometer) following the method of [Viollier et al. \(2000\)](#). Briefly, spectrophotometric analyses ($\lambda = 562$ nm) of the iron-ferrozine complexes were performed in a single aliquot before and after a reduction step with hydroxylamine. The procedure was calibrated using Fe(III) standards stable under normal conditions of analysis. The concentration of bulk dissolved Fe was also measured by MC-ICP-MS after separation by ion chromatography (see description below). The spectrophotometric and MC-ICP-MS methods provide nearly identical Fe(II) concentrations in the monimolimnion, demonstrating that Fe extraction yields by chromatography were always better than 95%.

Manganese concentrations were determined on filtered and acidified samples from the water column using ICP-AES (Perkin Elmer Optima 3000) at the Laboratory of Water Geochemistry, IGP. Sulfate (SO_4^{2-}) concentrations were measured by ion chromatography (Dionex DX-600 IC System) from filtered samples poisoned with zinc acetate to avoid reoxidation of any sulfide present. We also performed incubations to determine sulfate reduction rates using radiolabeled sulfate method ([Fossing and Jorgensen, 1989](#)).

2.4. Iron isotope analysis

Iron isotope compositions were determined on (1) water samples collected from various depths in the lake; (2) sediment core samples, specifically porewaters (bulk dissolved Fe), bulk solid Fe, highly reactive Fe, and pyrite Fe; and (3) volcanic rocks collected on outcrops of the Pavin crater. The extractions of reactive Fe and pyrite in sediments were performed following sequential extraction methods described previously ([Rouxel et al., 2005](#); [Severmann et al., 2006](#); [Fehr et al., 2008](#)). We chose to follow previous methods, despite alternative, more selective extraction schemes, to allow us to compare our results with those from other studies. Briefly, reactive Fe was leached using cold 1 M HCl for 3 h. This procedure extracted labile Fe phases such as amorphous Fe(III)-oxides, FeS, Fe-carbonates, and potentially some reactive silicate Fe. However, well-crystallized phases such as goethite, hematite, magnetite, and pyrite were not dissolved during this step. Following HCl treatment, Fe contained in pyrite was extracted using the sequential extraction method of [Huerta-Diaz and Morse \(1990\)](#). The residual sediment was treated in 10 N HF for 16 h to dissolve any silicate Fe, and this fraction was not analyzed further. After the HF step, the sediment residue was cleaned (with HCl and water rinses). Pyrite was assumed to be the only significant residual Fe phase after HCl and HF treatment ([Severmann et al., 2006](#)) and was extracted using concentrated HNO_3 overnight on a hotplate at ~ 120 °C. Although crystallized Fe(III) phases were not analyzed with this extraction scheme, they are a minor trace component of these sediments ([Viollier et al., 1997](#); [Schettler et al., 2007](#); [Cosmidis et al., 2014](#)).

Several papers have reported various experimental conditions to obtain the most precise and accurate Fe isotope analyses ([Beard and Johnson, 1999](#); [Malinovsky et al., 2003](#); [Weyer and Schwieters, 2003](#); [Dauphas et al., 2004, 2009](#); [Schoenberg and von Blanckenburg, 2005](#)). While the analysis of solid geological material has been widely explored (for example in [Beard and Johnson, 1999](#); [Malinovsky et al., 2003](#); [Schoenberg and von Blanckenburg, 2005](#)), no analytical tests for measurements of samples from anoxic waters have been published until now. In the present work, we aimed at (1) evaluate the precision and accuracy of our protocol used at the Geochemistry and Cosmochemistry Laboratory of the IPG Paris and (2) test potential Fe isotope fractionations related to anoxic water sampling. The Appendix A presents the detailed protocol for Fe isotope measurement as well as precision and accuracy estimated from long-term analyses of international standards. Briefly, the method can be summarized as follow. All solid samples were acidified with mixtures of HF, HCl, and/or HNO_3 to ensure (1) complete digestion and (2) that all Fe is in the ferric state. Iron was then separated from matrix elements on anion exchange chromatography in HCl medium ([Strelow, 1980](#); [Dauphas et al., 2004](#)). Iron concentrations and isotopic compositions were measured using a Neptune ThermoFischer MC-ICP-MS (Multiple Collector Inductively Coupled Plasma Mass Spectrometer). We corrected for instrumental mass discrimination using the conventional sample-standard bracketing (SSB) approach ([Belshaw et al., 2000](#); [Beard et al., 2003](#); [Rouxel et al., 2003](#); [Albarède and Beard, 2004](#)). The $^{56}\text{Fe}/^{54}\text{Fe}$ and $^{57}\text{Fe}/^{54}\text{Fe}$ ratios were expressed in the usual δ notation in per mil (‰) as:

$$\delta^{56}\text{Fe} = \left[\frac{(^{56}\text{Fe}/^{54}\text{Fe})_{\text{sample}}}{(^{56}\text{Fe}/^{54}\text{Fe})_{\text{standard}}} - 1 \right] \times 1000$$

and

$$\delta^{57}\text{Fe} = \left[\frac{(^{57}\text{Fe}/^{54}\text{Fe})_{\text{sample}}}{(^{57}\text{Fe}/^{54}\text{Fe})_{\text{standard}}} - 1 \right] \times 1000$$

where the standard is IRMM-014, from the Institute for Reference Materials and Measurements ([Taylor et al., 1992](#)). The analytical blank was always below 40 ng Fe (average ~ 30 ng) and represented less than 0.4% of the bulk Fe in samples. Based on replicate analyses of international rock standards over a 5-year period (see Appendix A), the external precision and accuracy were always better than 0.06‰ for $\delta^{56}\text{Fe}$ and 0.12‰ for $\delta^{57}\text{Fe}$ (2SD).

3. RESULTS

3.1. Water column

Results of the chemical and isotopic analyses on filtered water samples are given in [Table 1](#) and plotted in [Fig. 3](#). The concentration of dissolved ferrous iron in the oxic layer of the water column is low, with values < 0.1 μM . Because of this low concentration, no isotopic measurement was attempted for these samples. The concentration and isotopic composition of dissolved Fe in the anoxic zone both increase with depth in the water column, with values from less than 2 to more than 1200 μM and -2.14 ‰ to $+0.31$ ‰, respectively ([Table 1](#); [Fig. 3](#)). The strongest gradients in

Table 1

Dissolved manganese, sulfate and ferrous iron concentrations, together with isotopic composition of the bulk dissolved iron (expressed as $\delta^{56}\text{Fe}$ and $\delta^{57}\text{Fe}$), in water samples from Lac Pavin, collected in July 2007.

Sample #	Depth (m)	Mn(II) (μM)	SO_4^{2-} (μM)	Fe(II) (μM)	$\delta^{56}\text{Fe}$ (‰)	2SD (‰)	$\delta^{57}\text{Fe}$ (‰)	2SD (‰)
MX-15_8	55.0	0.08		0.0				
MX-15_9	56.0	0.09		0.0				
MX-15_10	57.0	0.42	14	0.0				
MX-15_11	57.5	0.29	14	0.0				
MX-15_12	58.0	0.31	14	0.1				
MX-15_13	58.5	1.65	14	0.0				
MX-15_14	59.0	2.39	15	0.0				
MX-15_15	59.5	7.49	14	0.1				
MX-15_16	60.0	14.9	14	2.1	-2.14	0.04	-3.16	0.06
MX-15_17	60.5	16.1	14	20.8	-1.30	0.08	-1.98	0.10
MX-15_18	61.0	17.4	14	106	-1.34	0.02	-1.97	0.08
MX-15_19	61.5	21.2	13	108	-1.25	0.04	-1.87	0.06
MX-15_20	62.0	19.6	9	174	-1.25	0.08	-1.84	0.08
MX-15_21	62.5	16.5	2	308	-0.51	0.04	-0.77	0.08
MX-15_22	63.0	15.7	4	378	-0.40	0.04	-0.58	0.06
MX-15_23	64.0	16.5	2	435	-0.33	0.06	-0.49	0.08
MX-15_24	65.0	16.7	1	470	-0.26	0.04	-0.38	0.08
MX-15_25	66.0	18.1	1	568	-0.15	0.04	-0.21	0.08
MX-15_26	68.0	19.0	1	688	-0.23	0.02	-0.33	0.10
MX-15_27	70.0	20.4	1	757	-0.11	0.04	-0.17	0.12
MX-15_28	72.0	21.2	2	864	-0.05	0.06	-0.06	0.12
MX-15_29	75.0	22.2		964	-0.01	0.08	0.00	0.14
MX-15_30	80.0	23.8		1004	0.23	0.04	0.34	0.12
MX-15_31	85.0	25.3		1074	0.20	0.06	0.28	0.18
MX-15_32	87.0	25.1		1105				
MX-15_33	89.0	26.4		1189				
MX-15_34	90.0	26.5		1210	0.31	0.08	0.45	0.12
MX-15_35	90.5	27.1		1203	0.31	0.08	0.48	0.08

Uncertainties correspond to 2SD (standard deviation).

Depth: depth in the water column. The oxic–anoxic interface is at 60 m depth.

dissolved Fe concentration and $\delta^{56}\text{Fe}$ values are in the depth range between 60 and 62.5 m. Sulfate concentrations are mostly constant around 14 μM in the oxic layer (data from 57 to 61 m, see also Fig. 2c) but decrease abruptly for depths deeper than 61.5 m. These concentration values are similar to those measured 20 years ago by Michard et al. (1994), indicating a long term stability of SO_4^{2-} level in the lake. The concentration of dissolved Mn(II) shows an increase with depth in the water column from 0.08 μM at a depth of 55 m to 27.1 μM in the deepest part of the lake. There is a peak of dissolved Mn(II) concentration located around 61.5 m depth (Fig. 3), suggesting that sinking Mn particles may be dissolved at that depth.

3.2. Sediments and porewaters

Iron concentrations and isotope compositions measured in sediments (bulk and sequential extractions) and associated porewaters are reported in Table 2 and Fig. 4. Iron concentrations in porewater of the four sediment cores are roughly constant within each individual core. However, comparison among the different cores show that the average Fe concentration increases with depth in the lake (Fig. 5a), with values of 30 ± 3 , 180 ± 70 , 510 ± 80 , 1170 ± 260 μM for cores at 32, 60, 65, and 92 m depth, respectively. The increase in Fe concentration with depth

tracks the increase of dissolved Fe concentration in the water column. The Fe concentration in bulk solid sediment also increases with depth below the sediment–water interface (Table 2). In order to avoid any dilution effect due to diatoms, organic matter, and detrital minerals deposition, it is preferable to trace authigenic Fe enrichment by using Fe/Al ratios rather than absolute Fe concentrations (e.g., Lyons and Severmann, 2006). The Fe/Al molar ratio in bulk sediment is significantly higher in the anoxic cores than in the oxic core, with average values of 0.21 ± 0.11 , 0.68 ± 0.32 , 0.84 ± 0.35 and 0.88 ± 0.37 for cores at 32, 60, 65 and 92 m depth, respectively (Fig. 5b). The Fe/Al ratio of the core in the oxic zone is lower than the average crustal value of 0.5 (e.g., Taylor and McLennan, 1995; Lyons and Severmann, 2006) but similar to the 0.3 ratio observed for volcanic rocks from Pavin catchment. In contrast, the three sediment cores sampled under anoxic waters at 60, 65, and 92 m are all significantly enriched in authigenic Fe, in good agreement with results from a previous study (Schettler et al., 2007).

The three sediment cores sampled under anoxic waters all show similar Fe isotope patterns among porewaters, bulk sediments, reactive Fe (cold HCl leach fraction), and pyrites. On average, porewaters, bulk sediment, and reactive Fe show $\delta^{56}\text{Fe}$ values near 0‰. In detail, mean $\delta^{56}\text{Fe}$ values of porewaters display a slight increase with depth, with

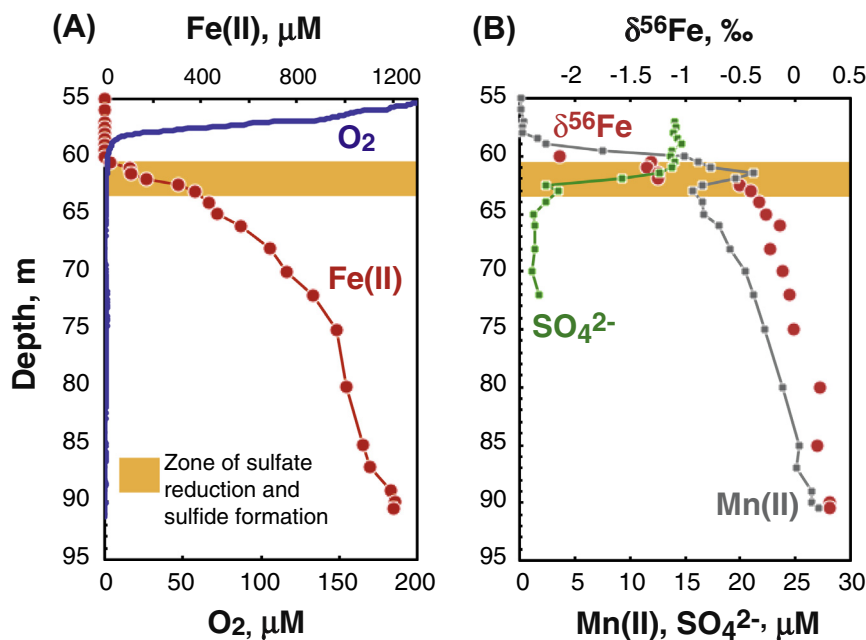


Fig. 3. Water column chemical profiles in Lac Pavin. (A) Dissolved oxygen and ferrous iron concentrations. (B) $\delta^{56}\text{Fe}$ value of dissolved iron together with manganese and sulfate concentrations. Below 60 m, the lake is anoxic and contains dissolved iron. There is a large shift in iron isotope values and iron concentrations, between 60 and 64 m, linked to ferrous iron oxidation. The limited iron isotope variability below 64 m is likely caused by ferric-ferrous interactions or limited amounts of water column iron reduction. Essentially all sulfate reduction and particulate sulfide formation in the lake occurs in the highlighted zone near the oxic–anoxic transition.

averages of $-0.08 \pm 0.13\text{‰}$ ($n = 6$), $0.02 \pm 0.07\text{‰}$ ($n = 9$), and $0.15 \pm 0.07\text{‰}$ ($n = 12$) for cores at 60, 65 and 92 m, respectively (Table 2). Bulk sediments have $\delta^{56}\text{Fe}$ values averaging $-0.10 \pm 0.11\text{‰}$ ($n = 4$), $0.11 \pm 0.20\text{‰}$ ($n = 12$), and $-0.02 \pm 0.12\text{‰}$ ($n = 13$) for cores at 60, 65 and 92 m, respectively. Reactive Fe averages $0.00 \pm 0.09\text{‰}$ ($n = 4$), $0.18 \pm 0.07\text{‰}$ ($n = 6$), and $-0.01 \pm 0.11\text{‰}$ ($n = 13$) for the cores at 60, 65 and 92 m, respectively. In contrast with these rather homogeneous values for porewaters, bulk sediment, and reactive Fe, $\delta^{56}\text{Fe}$ values of pyrites in sub-chemocline cores (60, 65 and 92 m) are highly variable and show significant deviations from the detrital iron isotope composition (overall $\delta^{56}\text{Fe}_{\text{pyrite}}$ between -1.51‰ and $+0.09\text{‰}$; average -0.93‰). For the individual cores, the average $\delta^{56}\text{Fe}$ values of pyrite are $-0.88 \pm 0.13\text{‰}$ ($n = 4$), $-0.61 \pm 0.39\text{‰}$ ($n = 7$), and $-1.20 \pm 0.24\text{‰}$ ($n = 9$) for cores at 60, 65 and 92 m, respectively. The core from the oxic zone is distinct from the sub-chemocline sediment cores, with pyrite $\delta^{56}\text{Fe}$ values that match the detrital iron flux ($\delta^{56}\text{Fe}_{\text{pyrite}}$ between -0.09‰ and $+0.26\text{‰}$, average $= 0.1 \pm 0.18\text{‰}$, $n = 4$). Importantly, a significant range of variation ($\sim 1\text{‰}$) for porewater $\delta^{56}\text{Fe}$ values in this core contrasts with the limited variability ($< 0.3\text{‰}$) observed for the sub-chemocline cores, where pyrite formation occurred in Fe-rich porewaters. The $\delta^{56}\text{Fe}$ of porewaters in sediments sampled from the oxic zone tend to increase with depth in the core, with values from -0.44‰ to $+0.64\text{‰}$ (Table 2; Fig. 4). This relationship is similar to that observed in sediments collected off California continental margin and probably reflects the effect of initial dissimilatory Fe reduction

with subsequent precipitation of Fe sulfides (Severmann et al., 2006).

3.3. Volcanic rocks from Lac Pavin

Iron concentrations and isotope compositions of the volcanic rocks are given in Table 3. They show a very homogeneous distribution, with Fe concentrations ranging from 5.81 to 6.66 wt% and $\delta^{56}\text{Fe}$ values from 0.16‰ to 0.22‰. Considering the analytical uncertainties, these are mostly constant Fe concentrations and $\delta^{56}\text{Fe}$ values, with an overall average for all samples at 6.41 ± 0.34 wt% and $0.20 \pm 0.02\text{‰}$ (1σ ; $n = 7$), respectively. For each sample, there is no difference in Fe concentration or $\delta^{56}\text{Fe}$ values between the different sub-samples (core vs. border vs. intermediate locations; Table 3). These data imply that alteration had no effect on bulk Fe budget in these rocks, although some redistribution within secondary mineral phases may have occurred. The $\delta^{56}\text{Fe}$ values of these volcanic rocks are similar to the average bulk values measured in our core collected at ~ 32 m depth in Lac Pavin below fully oxic waters (average $\sim 0.16 \pm 0.06\text{‰}$ [$n = 9$]; Table 2) but is slightly different from the average bulk values measured for subchemocline cores ($-0.10 \pm 0.11\text{‰}$ [$n = 4$], $0.11 \pm 0.20\text{‰}$ [$n = 12$], $-0.02 \pm 0.12\text{‰}$ [$n = 13$] for cores at 60, 65, and 92 m, respectively). The close similarity between $\delta^{56}\text{Fe}$ values of the volcanic rocks with those of sediments from Lac Pavin suggests that dominant authigenic phases present in the sediments (mostly vivianite and siderite) have $\delta^{56}\text{Fe}$ values close to the detrital input.

Table 2

Fe concentrations (in wt% for solid and in mM for porewater) and Fe isotope compositions in samples of the sediment cores collected in Lac Pavin.

Sample #	Sample type	Depth ^a (cm)	$\delta^{56}\text{Fe}$ (‰)	2SD (‰)	$\delta^{57}\text{Fe}$ (‰)	2SD (‰)	Fe conc (wt% or mM)	Fe/Al (molar)
<i>Core from the oxic layer (~32 m depth)</i>								
C3-1-1	Bulk	0	0.23	0.01	0.31	0.10	0.9	0.24
C3-2-1	Bulk	1.5	0.05	0.06	0.07	0.04		0.32
C3-3-1	Bulk	2.5	0.11	0.09	0.12	0.17	0.7	0.36
C3-4-1	Bulk	3.5	0.22	0.02	0.38	0.04	0.6	0.19
C3-5-1	Bulk	4.5	0.15	0.01	0.18	0.13	0.7	0.19
C3-6-1	Bulk	5.5	0.19	0.09	0.34	0.15	0.9	0.33
C3-7-1	Bulk	6.5	0.14	0.08	0.21	0.02	1.9	0.14
C3-8-1	Bulk	7.5	0.19	0.02	0.28	0.14	2.3	0.07
C3-9-1	Bulk	10	0.21	0.04	0.31	0.06	2.4	0.07
C3-1-1R	HCl leach	0	0.10	0.02	0.13	0.16	0.1	
C3-4-1R	HCl leach	3.5	0.07	0.08	0.12	0.14	0.1	
C3-8-1R	HCl leach	7.5	0.01	0.06	0.01	0.12	0.8	
C3-1-1P	Pyrite	0	0.26	0.08	0.33	0.12	0.1	
C3-2-1P	Pyrite	1.5	-0.09	0.04	-0.15	0.06	0.1	
C3-4-1P	Pyrite	3.5	0.25	0.06	0.36	0.10	0.2	
C3-8-1P	Pyrite	7.5	-0.01	0.09	-0.01	0.11	0.1	
C3-2-2	Porewater	1.5	-0.26	0.04	-0.41	0.10	0.04	
C3-3-2	Porewater	2.5	-0.44	0.06	-0.65	0.08	0.03	
C3-4-2	Porewater	3.5	-0.25	0.08	-0.41	0.06	0.04	
C3-5-2	Porewater	4.5	-0.06	0.09	-0.11	0.04	0.03	
C3-6-2	Porewater	5.5	0.13	0.04	0.18	0.16	0.03	
C3-7-2	Porewater	6.5	0.20	0.04	0.18	0.10	0.04	
C3-8-2	Porewater	7.5	0.64	0.02	0.90	0.15	0.03	
C3-9-2	Porewater	10	-0.09	0.06	-0.20	0.16	0.04	
<i>Core from the oxic–anoxic boundary (~60 m depth)</i>								
D-2	Bulk	2.75	-0.15	0.02	-0.23	0.06	0.60	0.94
F-2	Bulk	4.3	-0.20	0.02	-0.35	0.06	0.60	1.10
I-2	Bulk	9	-0.10	0.04	-0.09	0.10	0.70	0.32
L-2	Bulk	12.75	0.06	0.06	0.07	0.04	0.50	0.34
B-2R	HCl leach	0.85	0.10	0.01	0.17	0.06	0.40	
D-2R	HCl leach	2.75	-0.11	0.09	-0.16	0.04	0.50	
F-2R	HCl leach	4.3	0.03	0.04	0.05	0.10	0.20	
I-2R	HCl leach	9	-0.03	0.06	-0.05	0.17	0.30	
B-2P	Pyrite	0.85	-1.02	0.08	-1.51	0.10	0.20	
D-2P	Pyrite	2.75	-0.76	0.02	-1.17	0.13	0.20	
F-2P	Pyrite	4.3	-0.89	0.04	-1.38	0.12	0.04	
I-2P	Pyrite	9	-0.86	0.09	-1.29	0.04	0.04	
A-2	Porewater	0.85	-0.14	0.06	-0.25	0.08	0.05	
C-2	Porewater	2.75	-0.20	0.02	-0.27	0.02	0.20	
E-2	Porewater	4.3	-0.17	0.02	-0.25	0.06	0.22	
G-2	Porewater	5.9	0.03	0.04	0.02	0.08	0.23	
J-2	Porewater	9	0.13	0.04	0.13	0.10	0.18	
K-2	Porewater	12.75	-0.10	0.06	-0.10	0.06	0.20	
<i>Core from the anoxic layer (~65 m depth)</i>								
C2-1-1	Bulk	0	0.27	0.02	0.43	0.08	1.00	0.83
C2-2-1	Bulk	1.5	0.18	0.06	0.31	0.14	1.90	0.77
C2-3-1	Bulk	2.5	0.24	0.06	0.37	0.13	1.50	0.62
C2-4-1	Bulk	3.5	0.34	0.04	0.53	0.06	1.10	1.30
C2-5-2	Bulk	4.5	0.32	0.02	0.45	0.06	0.60	
C2-6-1	Bulk	5.5	0.25	0.04	0.40	0.06	0.60	0.85
C2-7-1	Bulk	6.5	0.09	0.04	0.15	0.06		1.46
C2-8-1	Bulk	7.5	0.19	0.04	0.27	0.08	0.80	1.16
C2-9-1	Bulk	8.5	-0.02	0.04	-0.05	0.04		0.82

(continued on next page)

Table 2 (continued)

Sample #	Sample type	Depth ^a (cm)	$\delta^{56}\text{Fe}$ (‰)	2SD (‰)	$\delta^{57}\text{Fe}$ (‰)	2SD (‰)	Fe conc (wt% or mM)	Fe/Al (molar)
C2-10-1	Bulk	9.5	-0.12	0.09	-0.22	0.14	1.10	0.58
C2-11-1	Bulk	10.5	-0.11	0.04	-0.18	0.02		0.51
C2-12-1	Bulk	11.5	-0.27	0.08	-0.39	0.12	1.50	0.29
C2-1-1R	HCl leach	0	0.21	0.02	0.33	0.16	0.80	
C2-2-1R	HCl leach	1.5	0.09	0.04	0.16	0.06	0.60	
C2-3-1R	HCl leach	2.5	0.13	0.09	0.20	0.04	0.60	
C2-5-1R	HCl leach	4.5	0.28	0.08	0.40	0.18	0.50	
C2-6-1R	HCl leach	5.5	0.24	0.09	0.37	0.12	0.50	
C2-10-1R	HCl leach	9.5	0.14	0.02	0.28	0.08	0.30	
C2-1-1P	Pyrite	0	-0.48	0.04	-0.83	0.10	0.10	
C2-2-1P	Pyrite	1.5	0.09	0.06	0.12	0.08	0.10	
C2-3-1P	Pyrite	2.5	-0.43	0.02	-0.69	0.02	0.02	
C2-4-1P	Pyrite	3.5	-0.56	0.04	-0.84	0.15	0.10	
C2-5-1P	Pyrite	4.5	-1.01	0.08	-1.53	0.08	0.09	
C2-6-1P	Pyrite	5.5	-0.84	0.02	-1.23	0.14	0.11	
C2-10-1P	Pyrite	9.5	-1.03	0.02	-1.50	0.12	0.15	
C2-1-2	Porewater	0	-0.12	0.06	-0.20	0.06	0.46	
C2-2-2	Porewater	1.5	0.01	0.06	-0.03	0.12	0.61	
C2-3-2	Porewater	2.5	0.03	0.04	0.06	0.10	0.41	
C2-4-2	Porewater	3.5	-0.01	0.06	-0.01	0.10	0.55	
C2-6-2	Porewater	5.5	0.03	0.04	0.06	0.09	0.63	
C2-7-2	Porewater	6.5	0.08	0.02	0.15	0.10	0.51	
C2-8-2	Porewater	7.5	-0.03	0.08	-0.05	0.19	0.56	
C2-9-2	Porewater	8.5	0.09	0.04	0.16	0.02	0.44	
C2-12-2	Porewater	11.5	0.09	0.04	0.13	0.08	0.46	
<i>Core at the bottom of Lac Pavin (~92 m depth)</i>								
1-1	Bulk	3.5	-0.06	0.06	-0.09	0.12	1.88	0.71
3-1	Bulk	8.5	0.15	0.04	0.20	0.08	2.70	1.18
5-1	Bulk	13.5	0.10	0.08	0.17	0.06	5.30	1.03
7-1	Bulk	18.5	-0.01	0.08	-0.09	0.04	2.20	0.79
9-1	Bulk	23.5	0.01	0.02	0.04	0.02	3.50	0.58
11-1	Bulk	28.5	-0.12	0.09	-0.22	0.16	6.70	0.88
13-1	Bulk	33.5	0.12	0.04	0.20	0.17	6.50	0.48
15-1	Bulk	38.5	-0.10	0.02	-0.21	0.04	6.50	0.46
17-1	Bulk	46	-0.15	0.06	-0.23	0.14	6.90	1.62
19-1	Bulk	51	0.08	0.02	0.09	0.06	7.10	0.60
21-1	Bulk	56	-0.19	0.06	-0.25	0.04	6.60	1.50
23-1	Bulk	63.5	0.01	0.02	0.02	0.08		0.73
25-1	Bulk	73.5	-0.15	0.06	-0.26	0.14	4.40	0.83
1-1R	HCl leach	3.5	-0.01	0.08	0.02	0.06		
3-1R	HCl leach	8.5	0.10	0.04	0.16	0.14	2.40	
5-1R	HCl leach	13.5	0.05	0.06	0.09	0.08	4.90	
7-1R	HCl leach	18.5	0.03	0.08	-0.06	0.10	1.60	
9-1R	HCl leach	23.5	0.00	0.06	0.02	0.06	3.40	
11-1R	HCl leach	28.5	0.06	0.02	0.09	0.06	6.00	
13-1R	HCl leach	33.5	0.04	0.08	0.10	0.10	3.80	
15-1R	HCl leach	38.5	-0.13	0.08	-0.20	0.15		
17-1R	HCl leach	46	-0.11	0.06	-0.20	0.04	6.50	
19-1R	HCl leach	51	0.19	0.06	0.24	0.14	6.30	
21-1R	HCl leach	56	-0.14	0.05	-0.19	0.14		
25-1R	HCl leach	73.5	-0.18	0.06	-0.28	0.06	0.40	
27-1R	HCl leach	83.5	-0.06	0.08	-0.11	0.08		
LPC-1	Pyrite	3.5	-1.08	0.07	-1.64	0.12	0.14	
LPC-2	Pyrite	5.5	-1.51	0.06	-2.25	0.12	0.02	
LPC-3	Pyrite	8.5	-0.78	0.02	-1.19	0.04	0.08	
LPC-4	Pyrite	10.5	-1.14	0.02	-1.75	0.06	0.55	
LPC-5	Pyrite	13.5	-1.14	0.04	-1.70	0.06	0.33	
LPC-6	Pyrite	15.5	-1.37	0.02	-2.00	0.04	0.39	

Table 2 (continued)

LPC-11	Pyrite	28.5	−1.00	0.02	−1.45	0.04	0.06
LPC-15	Pyrite	38.5	−1.28	0.02	−1.76	0.08	0.22
LPC-23	Pyrite	63.5	−1.48	0.04	−2.14	0.04	0.14
LPC-1-1	Porewater	3.5	0.09	0.15	0.01	0.04	1.41
LPC-5-2	Porewater	13.5	0.21	0.02	0.35	0.18	0.84
LPC-7-2	Porewater	18.5	0.04	0.02	0.09	0.10	0.86
LPC-11-2	Porewater	28.5	0.09	0.06	0.15	0.02	0.83
LPC-13-2	Porewater	33.5	0.09	0.02	0.26	0.12	0.90
LPC-15-2	Porewater	38.5	0.24	0.02	0.40	0.12	1.38
LPC-17-2	Porewater	46	0.12	0.04	0.20	0.04	1.31
LPC-19-2	Porewater	51	0.18	0.02	0.29	0.04	1.46
LPC-21-2	Porewater	56	0.16	0.02	0.26	0.10	1.48
LPC-23-2	Porewater	63.5	0.17	0.09	0.27	0.14	1.31
LPC-25-2	Porewater	73.5	0.18	0.08	0.31	0.04	1.23
LPC-27-2	Porewater	83.5	0.24	0.02	0.46	0.10	0.99
LPC-27-2	Porewater	83.5	0.24	0.02	0.46	0.10	0.99

Bulk: bulk Fe in solid sediment; HCl leach: reactive Fe representing easily soluble chemical species; pyrite: Fe extracted from the residue using HNO_3 treatment after sequential extraction (Severmann et al., 2006).

Uncertainties correspond to 2SD (standard deviation).

^a Depth in the sediment core. The water–sediment interface is at 0 cm depth.

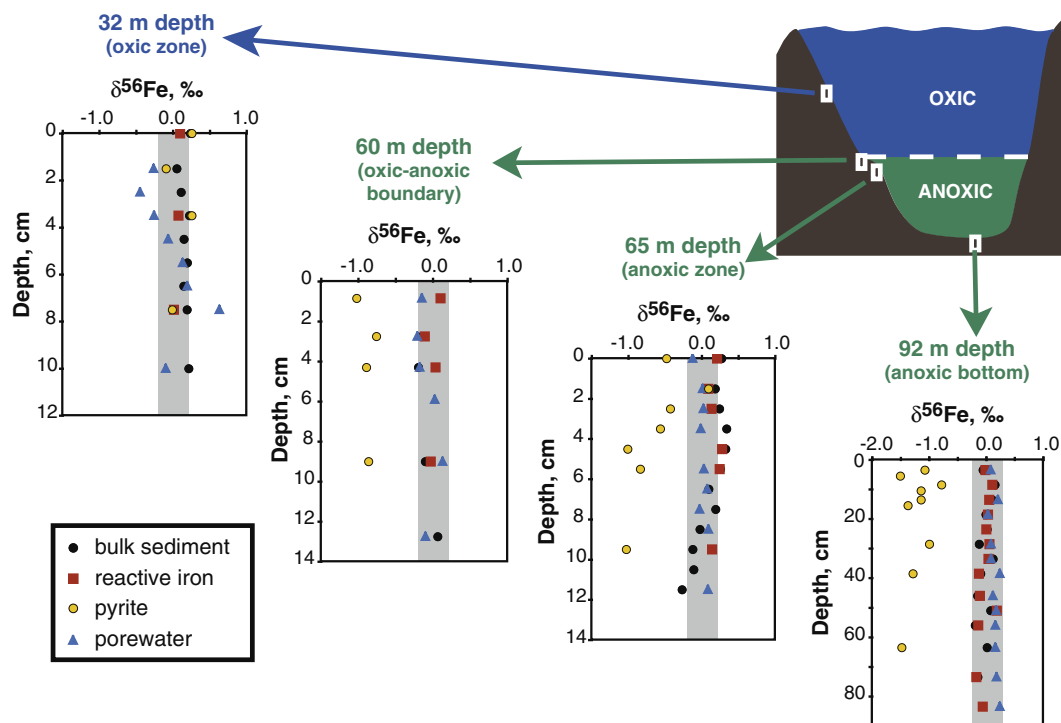


Fig. 4. Iron isotope composition of porewater, bulk rock, reactive iron, and pyrite in four sediment cores collected at Lac Pavin. Error bars on $\delta^{56}\text{Fe}$ values are smaller than dot sizes (typically $<0.03\text{‰}$, 1σ). There is limited isotope variability and deviations away from the detrital iron flux except for the sedimentary pyrite. The pyrite is isotopically variable and has $\delta^{56}\text{Fe}$ values similar to those seen in the zone near the oxic–anoxic transition in the water column where the majority of the iron sulfides form. For comparison, the vertical light-grey zones represent the typical range of Fe isotope compositions for detrital sediments, volcanic rocks and hydrothermal fluids.

4. DISCUSSION

4.1. Iron biogeochemical cycle in Lac Pavin

4.1.1. Iron cycling in the water column

Water samples in Lac Pavin show an increase, with increasing depth, in dissolved Fe concentration

(0.1–1200 μM) and $\delta^{56}\text{Fe}$ values (−2.14 to +0.31‰) (Fig. 3; Table 1). These results are similar to those obtained in two recent isotope studies focused on Fe cycling in other anoxic Fe-rich basins (Malinovsky et al., 2005; Teutsch et al., 2009). Malinovsky et al. (2005) examined Fe isotope variations in two lakes from Sweden affected by seasonally anoxic conditions. Iron isotope compositions of suspended

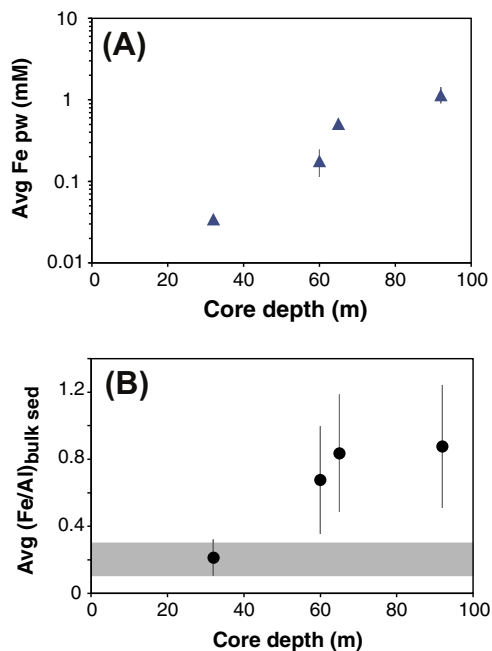


Fig. 5. Average Fe concentrations in porewaters (A) and Fe/Al molar ratio in bulk sediments (B) reported for each core as a function of the depth of the sediment core (32, 60, 65 and 92 m). Error bars on Y-axis represent standard deviation calculated for each core ($\pm 1\sigma$). Light grey zone in figure (B) indicates the range of Fe/Al ratios (0.1–0.3) of the volcanic rocks from the Pavin Crater, and is supposed to be representative of the detrital flux values, and is supposed to be representative of the detrital flux values, and is supposed to be representative of the detrital flux values. Fe/Al ratios higher than these detrital values result from an authigenic Fe enrichment of the sediment.

matter were found to be enriched in the heavy Fe isotope relative to dissolved Fe ($\sim 1\%$). The authors interpreted these results to reflect preferential partitioning of heavy isotopes during aqueous Fe(II) oxidation to Fe(III) and subsequent Fe(III) precipitation. Teutsch et al. (2009) measured the Fe contents and isotope compositions of the water column of meromictic Lake Nyoos (Cameroon). Iron contents and isotope compositions showed a strong increase with depth, with the highest gradient at the oxic–anoxic boundary. The very negative $\delta^{56}\text{Fe}$ values (-1.25%) observed for dissolved Fe at the oxic–anoxic boundary were tentatively interpreted to record intense dissimilatory iron reduction (DIR) from sinking Fe(III) particles previously formed at the surface of the lake. This interpretation is plausible since DIR can enrich Fe(II) in the light isotopes by $\sim 3\%$ relative to initial Fe(III) particles (Crosby et al., 2005). However, an assumption implicit in this model was that Fe oxidation was quantitative and occurring only when oxygen levels were $>1\ \mu\text{M}$. Therefore, the iron isotope profile in Lake Nyoos could also be driven by oxidation (Teutsch et al., 2009).

In Lac Pavin, oxidation generates the dissolved iron isotope gradient. Dissolved iron is mainly brought to the chemocline via diffusion from Fe-rich bottom waters (Michard et al., 1994). The oxidation of dissolved Fe(II) to Fe(III) at the chemocline enriches Fe(III) in the heavy isotopes by up to $\sim 3\%$, independent of whether this oxidation is biologically mediated or abiotic (Johnson et al., 2002; Welch et al., 2003; Jarzecki et al., 2004; Anbar et al., 2005; Balci et al., 2006). The precipitation of Fe(III) particles from dissolved Fe(II) produces either (1) no fractionation if the precipitation is slow or (2) possibly a kinetic isotope fractionation, enriching the solid in the light

Table 3

Iron concentrations and isotope compositions (expressed as $\delta^{56}\text{Fe}$ and $\delta^{57}\text{Fe}$) in volcanic rocks from Lac Pavin.

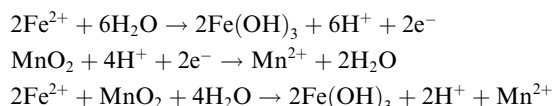
Sample	Sub-sample description	Analysis number	[Fe] (wt%)	$\delta^{56}\text{Fe}$ (‰)	2SD (‰)	$\delta^{57}\text{Fe}$ (‰)	2SD (‰)
RUD#1-C	Core	1	6.62	0.22	0.07	0.27	0.12
		2	5.64	0.21	0.07	0.31	0.11
		Avg	6.13	0.21		0.29	
RUD#1-B	Border	1	5.81	0.21	0.04	0.35	0.08
		2	5.80	0.21	0.03	0.35	0.04
		Avg	5.81	0.21		0.35	
RUD#2-C	Core	1	6.79	0.22	0.05	0.32	0.09
		2	5.90	0.16	0.01	0.28	0.06
		Avg	6.34	0.19		0.30	
RUD#2-B	Border	1	6.46	0.21	0.02	0.30	0.05
		2	6.87	0.17	0.05	0.27	0.05
		Avg	6.66	0.19		0.29	
RUD#3-C	Core	1	7.36	0.14	0.05	0.21	0.08
		2	5.90	0.18	0.04	0.28	0.11
		Avg	6.63	0.16		0.25	
RUD#3-M	Intermediate	1	6.95	0.19	0.06	0.27	0.12
		2	6.36	0.19	0.03	0.25	0.11
		Avg	6.66	0.19		0.26	
RUD#3-A	Altered surface	1	6.67	0.25	0.04	0.33	0.05
		2	6.61	0.19	0.04	0.27	0.01
		Avg	6.64	0.22		0.30	

Uncertainties correspond to 2SD (standard deviation).

Avg: average value of the two duplicate analyses for each sub-sample.

isotopes of Fe, if the reaction is rapid (Skulan et al., 2002). Overall, the net isotopic fractionation during Fe(III) particle formation from dissolved Fe(II) can thus be modulated by the rate of precipitation but, in most cases, it produces a precipitate enriched in the heavy isotopes of Fe. For instance, in experiments of abiotic precipitation of ferrihydrite from aqueous Fe(II), the precipitate is typically enriched in the heavy isotopes by $\sim 1\text{--}2\%$ (e.g., Bullen et al., 2001; Beard and Johnson, 2004). It is important to note that opposite Fe isotope fractionations have recently been found in water samples from anoxic Baltic Sea, where Fe(III) particles were depleted in heavy isotopes relative to the residual dissolved Fe (Staubwasser et al., 2013). This result was interpreted as due to a strong kinetic isotope fractionation during oxidation–precipitation process (Staubwasser et al., 2013).

The largest gradient of $\delta^{56}\text{Fe}$ values for dissolved Fe in the water column of Lac Pavin is observed near the chemocline, between 60 and 64 m depth, with the most negative values at 60 m. Oxygen levels are low ($< 2 \mu\text{M O}_2$) at that depth interval, suggesting microbial microaerophilic or anoxic pathways are the dominant modes of oxidation. Interestingly, this large gradient in $\delta^{56}\text{Fe}$ coincides with a significant increase in dissolved Mn concentration (Fig. 3), suggesting that part of the Fe(II) oxidation in this depth interval is coupled to Mn(IV) reduction. In detail, Fe(II) is oxidized to Fe(III) and precipitates as Fe oxyhydroxides (e.g., $\text{Fe}(\text{OH})_3$), while Mn(IV), initially present as MnO_2 particles, is reduced and thus solubilized to Mn(II). The overall reaction can be expressed as the following two half-reactions (Hongve, 1997):



Considering the reaction stoichiometry and the relative concentrations of dissolved Fe(II) and Mn(II) (Fig. 3), Mn(IV) reduction could be quantitatively driven by Fe(II) oxidation but the reverse appears impossible. There is too much Fe being oxidized (hundreds of $\mu\text{M/L}$) compared to Mn being reduced (tens of $\mu\text{M/L}$). Thus, another type of Fe oxidation is required either by microbial microaerophilic or anoxic oxidation. From 64 to 65 m, there is a subsequent Mn(II) drop, representing Mn sorption onto iron oxides or precipitation of other Mn-bearing mineral (Fig. 3).

Ferric precipitates formed at the redoxcline in Pavin may also include Fe(III)-phosphates due to particularly high concentrations of dissolved PO_4^{3-} in the monimolimnion (Cosmidis et al., 2014). In any case, the Mn(II) concentration profiles suggest that Fe isotope variations at 60–65 m depth is likely related to Fe oxidation rather than reduction. Molybdenum also shows significant decrease in this zone (Fig. 2c), which can be linked to adsorption on Mn oxides and Fe oxyhydroxides, and Mo coprecipitation with FeS (Viollier et al., 1995, 2014; Barling and Anbar, 2004). The sharp decrease in dissolved phosphate concentrations near the oxic–anoxic boundary (Fig. 2c) is likely also a signal for significant oxidation in this zone, since phosphate can strongly adsorb onto Fe oxide precipitates

(Buffle et al., 1989; Hongve, 1997; Konhauser et al., 2007). However, some phosphate is being removed in ferric Fe phosphates (Cosmidis et al., 2014).

Ferric particles formed at the chemocline sink in the water column down to the lake bottom. In contrast to Fe oxidation, microbial iron reduction at Lac Pavin occurs mostly in the sediment pile during early diagenesis rather than in the water column (Viollier et al., 1997). Porewater iron released to the water column is transported upward to the chemocline, predominantly through eddy diffusion (Aeschbach-Hertig et al., 1999).

Below 65 m, the increase with depth in the $\delta^{56}\text{Fe}$ values for dissolved iron is moderate compared to the sharp increase at the redox boundary (i.e., 60–64 m). This progressive $\delta^{56}\text{Fe}$ increase may derive from Fe isotope fractionation related to (1) adsorption of dissolved Fe(II) on Fe(III) particles formed at the chemocline (Icopini et al., 2004), (2) limited amount of iron reduction in the water column of the sinking Fe(III) particles (Beard and Johnson, 2004; Crosby et al., 2005) and/or (3) a putative isotopic effect due to ferrous phosphate (vivianite) precipitation in the deeper part of the water column, as evidenced from mineralogical data in the lake (Cosmidis et al., 2014). A contribution from a ferruginous sub-chemocline spring is also likely, and may explain part of the Fe isotope variability. The presence of a mineralized spring within the anoxic zone of Lake Pavin was proposed as early as 1975 in order to explain observed gradients at the redox boundary (Meybeck et al., 1975) and was hypothesized later from hydrological budgets and isotopic mass balances (Martin, 1985; Michard et al., 1994; Olive and Boulègue, 2004; Assayag et al., 2008; Jézéquel et al., 2011). Overall, observation of the lake level indicates a relative stability, within an uncertainty of ± 50 cm, over several decades (e.g. Assayag et al., 2008). Water inputs to the lake include direct precipitation (~ 18 L/S) and surface streams into the lake (~ 20 L/S) (Meybeck et al., 1975; Martin, 1985; Aeschbach-Hertig et al., 2002). Water outputs are dominated by evaporation (~ 7 L/s) and surface outlet flowing into the Couze Pavin river (on average ~ 50 L/s) (Meybeck et al., 1975; Martin, 1985; Aeschbach-Hertig et al., 2002; Assayag et al., 2008). Thus, the difference between water inputs and outputs leads to a deficit of about 20 L/s (Aeschbach-Hertig et al., 1999, 2002), which is assumed to be balanced by sub-surface springs (Glangeaud, 1916; Meybeck et al., 1975; Martin, 1985; Viollier et al., 1997; Aeschbach-Hertig et al., 1999, 2002; Olive and Boulègue, 2004; Assayag et al., 2008; Jézéquel et al., 2011). The main question concerns the distribution and nature of these sub-surface springs in the mixolimnion and monimolimnion. High precision and high frequency temperature and conductivity profiles recently confirmed the presence of a sub-lacustrine, intermittent cold spring at the bottom of the mixolimnion at depth between 50 and 55 m (Bonhomme et al., 2011), as earlier detected in a previous study (Aeschbach-Hertig et al., 2002). In the monimolimnion, a deep ferruginous spring is clearly required to feed and sustain high Fe concentrations in the anoxic water layer, especially considering the high Fe removal flux through burial in the sediments deposited under anoxic waters. The precise depth of this purported

ferruginous spring is unknown but has been hypothesized to be located at the lake bottom (Michard et al., 1994; Assayag et al., 2008) or in the upper part of the monimolimnion at ~65 m (Jézéquel et al., 2011). In terms of Fe isotopes, there is a slight shift towards negative $\delta^{56}\text{Fe}$ values at ~68 m depth, which may confirm a deep spring input at that depth (Fig. 2b).

4.1.2. Iron isotope signature of sedimentary pyrite inherited from water column cycling

In theory, negative $\delta^{56}\text{Fe}$ values in pyrite can be explained by three different scenarios: (1) Fe isotope fractionation associated with DIR in the sediment, releasing preferentially light Fe in the porewaters and subsequent incorporation of this Fe into diagenetic pyrite (e.g., Johnson et al., 2008b); (2) Fe isotope fractionation related to diagenetic pyrite formation from porewater Fe(II) (e.g., Guilbaud et al., 2011); and (3) pelagic pyrite formation in depth intervals where Fe(II) is driven light as a result of partial oxidation (e.g., Rouxel et al., 2005). These three scenarios are explored in detail below with regard to the present Pavin data.

First, if the light $\delta^{56}\text{Fe}$ values of pyrite were linked to DIR, porewater $\delta^{56}\text{Fe}$ values need to be significantly negative, with values similar to those of pyrite, around -0.9‰ . This is clearly not the case; porewaters in sub-chemocline cores have $\delta^{56}\text{Fe}$ values near 0‰ (Table 2), indicating that DIR is not the process driving to negative $\delta^{56}\text{Fe}$ values in pyrite. It must be noted that very high Fe concentrations in porewaters attest to extensive DIR (average Fe concentrations of 180 ± 70 , 510 ± 80 , $1170 \pm 260 \mu\text{M}$ for cores at 60, 65, and 92 m, respectively; Table 2 and Fig. 5a). The iron isotope fractionation typically associated with DIR is likely not expressed in these porewaters because Fe reduction is complete, similar to what is expected in continental margin marine sediments where limited iron flux is associated with high organic matter content.

The second scenario implies that negative $\delta^{56}\text{Fe}$ recorded in pyrite results from Fe isotope fractionation associated with its precipitation either in the water column or in the sediment. Experimental studies show that a depletion of -2.2‰ in pyrite can be produced during formation from aqueous Fe^{2+} (Guilbaud et al., 2011). However, estimates of the isotopic effects of this process range from kinetically controlled fractionations that enrich pyrite in the light Fe isotopes (e.g., Severmann et al., 2006; Guilbaud et al., 2011), to equilibrium fractionations, which yield pyrite extensively enriched in heavy isotopes (e.g., Polyakov et al., 2007). One of the main pyrite precursor, mackinawite (FeS), is also affected by kinetic Fe isotope fractionation when precipitated at low pH (~4; Butler et al., 2005; Guilbaud et al., 2010) but can reach equilibrium, with an enrichment in heavy Fe isotopes, at near-neutral pH conditions (Wu et al., 2012). At Lac Pavin, the presence of pyrite with near crustal values in the oxic core (32 m), where pyrite formation occurs in porewaters with moderate dissolved ferrous iron concentrations ($>30 \mu\text{M}$ Fe(II)) and low extent of pyritization, is not consistent with presence of large kinetic fractionations in low temperature ferruginous aqueous systems. Additionally, assuming that Fe isotope

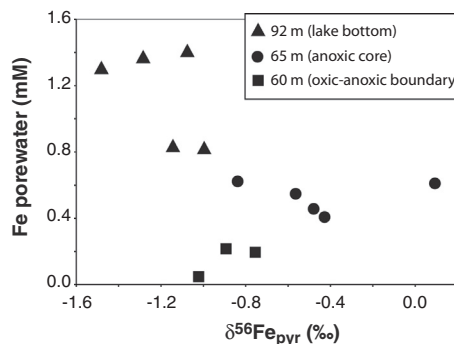


Fig. 6. Iron concentration in porewaters reported as a function of Fe isotope composition of pyrite for anoxic sediment cores.

composition of sedimentary pyrite is controlled by kinetic isotope fractionation during precipitation of pyrite in the anoxic sediment cores, one might predict a relationship between Fe concentrations in sediment porewater and pyrite $\delta^{56}\text{Fe}$ values. Interestingly, this is not observed; there is no clear trend between these two parameters in the anoxic sediment cores (Fig. 6). The range of pyrite $\delta^{56}\text{Fe}$ values for the various sediment cores overlap (around -1‰) while porewater Fe concentrations show strong variability, increasing with depth in the water column. We therefore suggest that pyrite $\delta^{56}\text{Fe}$ values in Lac Pavin sediments do not reflect a kinetic isotope fractionation. However, our conclusion would only apply to ferruginous systems and it is not in agreement with previous results obtained on pyrites from sulfate- and sulfide rich sediments in California, which suggest that the apparent Fe isotope fractionation between aqueous Fe^{2+} and pyrite was $>1.5\text{‰}$ (Severmann et al., 2006). The discrepancy between the various data published so far (either calculated, determined experimentally or from natural systems) may reflect strong pathway dependence of the isotopic fractionations involved in pyrite formation.

At Lac Pavin, negative and highly variable pyrite $\delta^{56}\text{Fe}$ values in sub-chemocline cores may reflect that pyrite Fe was sourced from an Fe(II) pool with variable and depleted $\delta^{56}\text{Fe}$ values. In Lac Pavin, such variability and depletion only occurs in the water column within the vicinity of the oxycline. We propose that Fe-sulfides form in the water column at the oxic–anoxic boundary (~60 m depth) and transfer their Fe isotope signature to sedimentary pyrite with limited post formation iron isotope fractionation. Water column profiles show that sulfate reduction occurs within the redox boundary (61–65 m depth), where the Fe isotope gradient is the strongest (Table 1, Fig. 3b). Below these depths sulfide concentrations are controlled by FeS solubility and sulfate levels are constant, presumably at concentrations below what microbial sulfate reducers can utilize. Consistent with this view, we found sulfate reduction rates of $<10^{-3} \mu\text{mol L}^{-1} \text{d}^{-1}$ at 55 m (oxic waters) and 70 m depth, but notably higher rates ($2 \times 10^{-3} \mu\text{mol L}^{-1} \text{d}^{-1}$) at 61 m, confirming that bacterial sulfate reduction occurs mainly at the redox boundary and is restricted there by the availability of sulfate. This scenario is supported by the results from a previous study on reduced sulfur species distribution in the anoxic water column of Lac Pavin

(Bura-Nakic et al., 2009). From a comparison between traditional and voltammetry S data, this study demonstrated that free $\text{H}_2\text{S}/\text{HS}^-$ concentrations are extremely low and about 80% of the total sulfide occurs as iron sulfide colloids. Therefore, constraints on water column S cycling indicate that particulate iron sulfide formation occurs near the chemocline. The idea that pyrite in the anoxic cores tracks the dissolved iron isotope values of the zone of particulate iron sulfide formation near the chemocline is corroborated by the similarity between the Fe isotope compositions found in sediment pyrites (Fig. 4) and dissolved Fe(II) at the oxic–anoxic interface (Fig. 3b).

Down-core variability in pyrite $\delta^{56}\text{Fe}$ values over short distances can be explained by expansion and contraction of the thickness of the zone of iron oxidation in the water column and the relative depth of water-column sulfate reduction and FeS formation with respect to the $\delta^{56}\text{Fe}$ gradient. For instance, when oxic shallow waters are affected by seasonal mixing down to 60 m depth, the iron gradient at the chemocline is sharpened both in concentration and isotope composition. This condition affects the $\delta^{56}\text{Fe}$ values of dissolved iron in the zone where the majority of sulfides form (Bura-Nakic et al., 2009). As noted above, the large variability in sediment pyrite values are difficult to explain if pyrite Fe isotope composition is inherited within the sediment, given mostly constant porewater Fe concentration and isotope profiles. We cannot, however, completely rule out with current constraints that below the chemocline there is porewater pyrite formation from FeS precursors and that this process involves an isotope fractionation (e.g., Severmann et al., 2006).

From X-ray diffraction (XRD) and Scanning Electron Microscopy (SEM) analyses of Lac Pavin sediments, Viollier et al. (1997) identified spherical aggregates (20–30 μm) of bipyramidal pyrite crystals (0.5–1 μm) termed framboids. These authors suggested that pyrite could form after diagenetic dissolution of proto-vivianite (ferrous phosphate) in the sediment because they were not able to find any phosphate particles in their sediment sample. This hypothesis is clearly not supported by latter studies, showing that vivianite is the main authigenic mineral in Lac Pavin sediments, with concentrations representing up to 70 wt% of the total sediment (Schettler et al., 2007; Cosmidis et al., 2014). In a recent and more detailed mineralogical study of Lac Pavin, pyrite was not readily identified by SEM or Transmission Electron Microscopy (TEM) techniques in either particulate matter from the water column or surface sediments (Cosmidis et al., 2014). This is likely due to the very low abundance of pyrite in these samples (<0.2 wt%; see also Table 2) relative to diatoms, ferric and ferrous phosphate and organic matter (dilution effect). Consistent with this view, the authors noted that EXAFS (Extended X-ray Absorption Fine Structure) spectra obtained from synchrotron-based analyses were better fitted by addition of pyrite, particularly in a sediment trap placed at 67 m in the water column (just below the sulfate reduction zone). Better constraints on the extents porewater and water column pyrite formation at Lac Pavin are, therefore, required to incontrovertibly link sediment pyrite values with water column iron cycling.

4.2. Implications for Archean environment and biosphere

Work at Lac Pavin can help to improve our foundation for interpreting the sedimentary iron isotope record over geologic time (Fig. 1). There is not strong evidence at Lac Pavin for large kinetic iron isotope fractionations during pyrite formation under iron-rich conditions. We suggest that our observations at Pavin can be broadly applied to other ferruginous systems, modern and ancient. Iron isotope variability at Pavin is most easily linked to iron redox cycling within the water column. Specifically, oxidation of a large dissolved iron pool is the main process that induces iron isotope variability within the water column, and some of this variability is likely transferred to the sediments via iron sulfide formation in the water column. Since there is a discrete redoxcline at Pavin, with fully oxic surface waters above, there is ultimately quantitative oxidation and limited isotope variability in the bulk sediment.

Using Lac Pavin as a guide, the oxidative side of the iron cycle likely imparted iron isotope variability to the Archean sedimentary record. Work at Pavin supports the model that enhanced sedimentary iron isotope variability in the Neoproterozoic is linked to an extensive oxidative iron cycle but one in which partial oxidation prevailed in broad swaths of the shallow ocean. In this model, non-quantitative behavior is the key to inducing large sediment iron isotope variability (Rouxel et al., 2005). Before the permanent rise of atmospheric oxygen [2.5–2.3 Ga (Bekker et al., 2004; Konhauser et al., 2011)], iron oxidation in an upwelling water mass could have been a protracted, incomplete process—allowing for burial of iron oxides with positive $\delta^{56}\text{Fe}$ values and leaving behind an isotopically depleted dissolved iron reservoir that could be transferred to the sedimentary record with or without associated fractionations (as pyrite, carbonate or iron oxides). From this perspective, the decrease in iron isotope variability in the sedimentary record around 2.45 billion years ago (Rouxel et al., 2005; Johnson et al., 2008b) marks the first full-scale and persistent oxidation of the upper ocean. We further propose that the appearance of pronounced negative iron isotope values in the sedimentary record around 3.0 billion years ago, compared to heavy or near crustal values that seem to characterize the earlier sedimentary iron isotope record (Fig. 1) reflect the first onset of large-scale partial oxidation of iron in response to an important evolution of photosynthetic machinery. Photosynthesis, either oxygenic or anoxygenic (Cloud, 1973; Kappler et al., 2005), are likely to provide means to oxidize the extensive amount of iron (>50% of dissolved iron pool) needed to cause large iron isotope gradients (Rouxel et al., 2005). Locally, dissimilatory Fe reduction in sediment porewater and associated diagenetic reactions may have further enhanced Fe isotope variability in marine sediments. For instance, earlier studies based on C and Fe isotope compositions suggested that Fe cycling recorded in Archean carbonates largely reflect dissimilatory iron reduction (Heimann et al., 2010; Craddock and Dauphas, 2011). Using Lac Pavin as a guide, however, it seems an oxidation model can explain a large part of the iron isotope variability observed in the Archean sediments. Banded Iron Formations have a large range of $\delta^{56}\text{Fe}$ values with

markedly positive and negative $\delta^{56}\text{Fe}$ values (Fig. 1). This range can reflect partial oxidation and distillation of the dissolved Fe reservoir due to progressive removal of Fe oxides to the sediment (e.g. Rouxel et al., 2005; Tsikos et al., 2010). Pyrites measured so far in Archean rocks are generally contained in organic-rich sediments. In these settings, one can expect extensive sediment microbial Fe reduction with limited Fe isotope fractionation, similar to what we observed in Lac Pavin.

If we are correct, then the Archean data would fingerprint a fundamental shift in the oxidative capacity of the ocean. This capacity would be regulated by photosynthesis. Therefore, we propose that the sedimentary iron isotope record pinpoints the timing of one of the most significant biological evolutionary events in Earth's history—the ability of organisms to utilize sunlight to mediate electron transfer—at ~ 3.0 Ga. Recently, novel phylogenomic approaches looking at the collective evolutionary record of gene families and protein domain structures have suggested a period of rapid evolutionary innovation during a genetic expansion around 3.0 Ga (David and Alm, 2011; Wang et al., 2011). More focused phylogenomic reconstructions suggest the emergence of cyanobacteria in the Mesoarchean (Schirrmeister et al., 2013), contemporaneous with the first appearance of appreciable atmospheric oxygen (Crowe et al., 2013). Our work hints at a convergence in molecular and geochemical estimates for the timing of the first major diversification of life on Earth and the ability of organisms to use sunlight to fuel electron transfer.

5. SUMMARY

The present study shows strong dissolved iron isotope variability in the water column of anoxic and ferruginous Lac Pavin, with $\delta^{56}\text{Fe}$ values ranging from -2.1‰ to $+0.3\text{‰}$. The low $\delta^{56}\text{Fe}$ values and strong Fe isotope gradient observed close to the oxic–anoxic boundary reflect the effect of Fe oxidation and precipitation, leaving residual ferrous iron depleted in heavy isotopes.

Compared with water column, there is limited Fe isotope variability in sediment porewaters, bulk sediments, and reactive Fe, with $\delta^{56}\text{Fe}$ values essentially near 0‰ . The largest range of $\delta^{56}\text{Fe}$ in sediments is found in pyrites, with values between -1.51‰ and $+0.09\text{‰}$; average -0.93‰ , similar to those measured in dissolved iron at the oxic–anoxic boundary of the water column. We suggest that iron sulfides precipitate at the redox boundary where sulfate is reduced to sulfide and that these sulfides record the Fe isotope variability of the chemocline. However, we cannot completely rule out porewater pyrite formation, which could have had an accompanying kinetic iron isotope fractionation. The limited iron isotope variability in porewaters, bulk sediments, and reactive Fe is linked to near quantitative oxidation at chemocline and quantitative microbial iron reduction in porewaters. In Lac Pavin, there is not clear Fe isotope signal for microbial iron reduction.

Using Lac Pavin as a guide for interpreting Archean records of ferruginous oceans, these findings support that variable and markedly negative iron isotopes values in sedimentary pyrites and shales in the Archean reflect partial

ferrous iron oxidation in the water column and capture of remaining isotopically light reservoir (Rouxel et al., 2005). Before the large-scale rise of atmospheric oxygen around the Great Oxidation Event at ~ 2.4 Ga iron oxidation in upwelling water masses could have been a protracted process—allowing for burial of iron oxides with positive $\delta^{56}\text{Fe}$ values and leaving behind an isotopically depleted dissolved iron reservoir (Rouxel et al., 2005). With the establishment of a discrete redoxcline in the oceans quantitative iron oxidation would have prevailed. Thus oxidation of the surface oceans would have prevented efficient separation of ferric oxides with positive $\delta^{56}\text{Fe}$ values from the dissolved negative residue. In this light, the iron isotope record provides support for the presence of only restricted ‘oxygen oasis’ in the Archean rather than a fully oxic surface layer. Partial oxidation would be most likely in water masses with high rates of both upwelling and lateral transport, which is consistent with the presence of the lightest sedimentary iron isotope values in highly organic rich systems that would be fed by a strong nutrient fluxes (Rouxel et al., 2005). Linking the iron isotope record to redox evolution provides a simple explanation for why sulfidic, organic matter-rich shales, a sedimentary rock type relatively common throughout the Earth's history, would have unusually negative Fe isotope values prior to the rise of atmospheric oxygen around 2.4 billion years ago.

ACKNOWLEDGMENTS

This work was partly funded by the ANR-EC2CO (META-NOX project) and by the BQR program of IPGP. We are thankful to Gil Michard, Magali Ader, Oanez Lebeau, Patrick Alberic, Olivier Rouxel, Anne-Catherine Lehours, Corinne Biderre-Petit, Julie Cosmidis, Karim Benzerara, Donald Canfield, and Guillaume Morin for constructive discussions. Yves Gamblin and Antonio Vieira from the IPGP mechanics workshop are thanked for producing the 1 L syringe-based water sampler. The University Blaise Pascal of Clermont-Ferrand allowed the use of Besse biological station nearby the lake and provided boats and platform. The US National Science Foundation (EAR-PF) and NASA Exobiology and Astrobiology programs supported the work of Planavsky and Lyons.

APPENDIX A. SUPPLEMENTARY DATA

Supplementary data associated with this article can be found, in the online version, at <http://dx.doi.org/10.1016/j.gca.2014.03.004>.

REFERENCES

- Aeschbach-Hertig W., Hofer M., Kipfer R., Imboden D. I. and Wieler R. (1999) Accumulation of mantle gases in a permanently stratified volcanic lake (Lac Pavin, France). *Geochim. Cosmochim. Acta* **63**, 3357–3372.
- Aeschbach-Hertig W., Hofer M., Schmid M., Kipfer R. and Imboden D. M. (2002) The physical structure and dynamics of a deep, meromictic crater lake (Lac Pavin, France). *Hydrobiologia* **487**, 111–136.
- Albarède F. and Beard B. L. (2004) Analytical methods for non-traditional isotopes. In *Geochemistry of Non-Traditional Stable*

- Isotopes* (eds. C. M. Johnson, B. L. Beard and F. Albarède). Mineralogical Society of America and Geochemical Society, Washington, DC, pp. 113–152.
- Amblard C. and Bourdier G. (1990) The spring bloom of the diatom *Melosira italica* subsp. *subarctica* in Lake Pavin: biochemical, energetic and metabolic aspects during sedimentation. *J. Plank. Res.* **12**, 645–651.
- Anbar A. D., Jarzecki A. A. and Spiro T. G. (2005) Theoretical investigation of iron isotope fractionation between $\text{Fe}(\text{H}_2\text{O})_6^{3+}$ and $\text{Fe}(\text{H}_2\text{O})_6^{2+}$: implications for iron stable isotope geochemistry. *Geochim. Cosmochim. Acta* **69**, 825–837.
- Anbar A. and Rouxel O. (2007) Metal stable isotopes in paleoceanography. *Annu. Rev. Earth Planet. Sci.* **35**, 717–746.
- Archer C. and Vance D. (2006) Coupled Fe and S isotope evidence for Archean microbial Fe(III) and sulfate reduction. *Geology* **34**, 153–156.
- Assayag N., Jézéquel D., Ader M., Viollier E., Michard G., Prévot F. and Agrinier P. (2008) Hydrological budget, carbon sources and biogeochemical processes in Lac Pavin (France): constraints from ($\delta^{18}\text{O}$ of water and $\delta^{13}\text{C}$ of dissolved inorganic carbon). *Appl. Geochem.* **23**, 2800–2816.
- Balci N., Bullen T. D., Witte-Lien K., Shanks W. C., Motelica M. and Mandernack K. W. (2006) Iron isotope fractionation during microbially stimulated Fe(II) oxidation and Fe(III) precipitation. *Geochim. Cosmochim. Acta* **70**, 622–639.
- Barling J. and Anbar A. D. (2004) Molybdenum isotope fractionation during adsorption by manganese oxides. *Earth Planet. Sci. Lett.* **217**, 315–329.
- Beard B. L. and Johnson C. M. (1999) High precision iron isotope measurements of terrestrial and lunar materials. *Geochim. Cosmochim. Acta* **63**, 1653–1660.
- Beard B.L. and Johnson C.M. (2004) Fe isotope variations in the modern and ancient Earth and other planetary bodies. In: C.M. Johnson, B.L. Beard and F. Albarède (Editors), *Geochemistry of non-traditional stable isotopes. Reviews in Mineralogy and Geochemistry*. Mineralogical Society of America and Geochemical Society, Washington DC., pp. 319–357.
- Beard B. L., Johnson C. M., Skulan J. L., Nealon K. H., Cox L. and Sun H. (2003) Application of Fe isotopes to tracing the geochemical and biological cycling of Fe. *Chem. Geol.* **195**, 87–117.
- Bekker A., Holland H. D., Wang P. L., Rumble D., Stein H. J., Hannah J. L., Coetzee L. L. and Beukes N. J. (2004) Dating the rise of atmospheric oxygen. *Nature* **427**, 117–120.
- Belshaw N. S., Zhu X. K. and O’Nions R. K. (2000) High precision measurement of iron isotopes by plasma source mass spectrometry. *Int. J. Mass Spectrom.* **197**, 191–195.
- Beukes N. J. and Gutzmer J. (2008) Origin and Paleoenvironmental significance of major iron formations at the Archean–Paleoproterozoic boundary. *Soc. Econ. Geol. Rev.* **15**, 5–47.
- Biderre-Petit C., Jézéquel D., Dugat-Bony E., Lopes F., Kuever J., Borrel G., Viollier E., Fonty G. and Peyret P. (2011) Identification of microbial communities involved in the methane cycle of a freshwater meromictic lake. *FEMS Microbiol. Ecol.* **77**, 533–545.
- Bonhomme C., Poulin M., Vinçon-Leite B., Saad M., Groleau A., Jézéquel D. and Tassin B. (2011) Maintaining meromixis in Lake Pavin (Auvergne, France): the key role of a sublacustrine spring. *C. R. Geosci.* **343**, 749–759.
- Buffle J., De Vitre R. R., Perret D. and Leppard G. G. (1989) Physico-chemical characteristic of a colloidal iron phosphate species formed at the oxic-anoxic interface of a eutrophic lake. *Geochim. Cosmochim. Acta* **53**, 399–408.
- Bullen T. D., White A. F., Childs C. W., Vivit D. V. and Schulz M. S. (2001) Demonstration of significant abiotic iron isotope fractionation in nature. *Geology* **29**, 699–702.
- Bura-Nakic E., Viollier E., Jézéquel D., Thiam A. and Ciglenecki I. (2009) Reduced sulfur and iron species in anoxic water column of meromictic crater Lake Pavin (Massif Central, France). *Chem. Geol.* **266**, 320–326.
- Butler I. B., Archer C., Vance D., Oldroyd A. and Rickard D. (2005) Fe isotope fractionation on FeS formation in ambient aqueous solution. *Earth Planet. Sci. Lett.* **236**, 430–442.
- Busigny V. and Dauphas N. (2007) Tracing paleofluid circulations using iron isotopes: a study of hematite and goethite concretions from the Navajo Sandstone (Utah, USA). *Earth Planet. Sci. Lett.* **254**, 272–287.
- Chapron E., Albéric P., Jézéquel D., Versteeg W., Bourdier J.-L. and Sitbon J. (2010) Multidisciplinary characterisation of sedimentary processes in a recent maar lake (Lake Pavin, French Massif Central) and implication for natural hazards. *Nat. Hazards Earth Syst. Sci.* **10**, 1815–1827.
- Cloud P. (1973) Paleocological significance of banded iron-formation. *Econ. Geol.* **68**, 1135–1143.
- Cosmidis J., Benzerara K., Morin G., Busigny V., Lebeau O., Jézéquel D., Noël V., Dublet G. and Othmane G. (2014) Biomineralization of mixed valence iron-phosphates in the anoxic water column of Lake Pavin (Massif Central, France). *Geochim. Cosmochim. Acta* **126**, 78–96.
- Craddock P. R. and Dauphas N. (2011) Iron and carbon isotope evidence for microbial iron respiration throughout the Archean. *Earth Planet. Sci. Lett.* **303**, 121–132.
- Crosby H. A., Johnson C. M., Roden E. E. and Beard B. L. (2005) Coupled Fe(II)–Fe(III) electron and atom exchange as a mechanism for Fe isotope fractionation during dissimilatory iron oxide reduction. *Environ. Sci. Technol.* **39**, 6698–6704.
- Crowe S. A., Døssing L. N., Beukes N. J., Bau M., Kruger S. J., Frei R. and Canfield D. E. (2013) Atmospheric Oxygen 3.0 billion years ago. *Nature* **501**, 535–538.
- Czaja A. D., Johnson C. M., Roden E. E., Beard B. L., Voegelin A. R., Nägler T. F., Beukes N. J. and Wille M. (2012) Evidence for free oxygen in the Neoproterozoic ocean based on coupled iron-molybdenum isotope fractionation. *Geochim. Cosmochim. Acta* **86**, 118–137.
- Dauphas N., Janney P. E., Mendybaev R. A., Wadhwa M., Richter F., Davis A. M., van Zuilen M., Hines R. and Foley C. N. (2004) Chromatographic separation and multicollection-ICPMS analysis of iron – investigating mass-dependent and -independent isotope effects. *Anal. Chem.* **76**, 5855–5863.
- Dauphas N. and Rouxel O. J. (2006) Mass spectrometry and natural variations of iron isotopes. *Mass. Spectrom. Rev.* **25**, 515–550.
- Dauphas N., Cates N. L., Mojzsis S. J. and Busigny V. (2007a) Identification of chemical sedimentary protoliths using iron isotopes in the >3750 Ma Nuvvuagittuq supracrustal belt, Canada. *Earth Planet. Sci. Lett.* **254**, 358–376.
- Dauphas N., van Zuilen M., Busigny V., Lepland A., Wadhwa M. and Janney P. E. (2007b) Iron isotope, major and trace element characterization of early Archean supracrustal rocks from SW Greenland: Protolith identification and metamorphic overprint. *Geochim. Cosmochim. Acta* **71**, 4745–4770.
- Dauphas N., Pourmand A. and Teng F.-Z. (2009) Routine isotopic analysis of iron by HR-MC-ICPMS: how precise and how accurate? *Chem. Geol.* **267**, 175–184.
- David L. A. and Alm E. J. (2011) Rapid evolutionary innovation during an Archean genetic expansion. *Nature* **469**, 93–96.
- Duan Y., Severmann S., Anbar A., Lyons T. W., Gordon G. W. and Sageman B. B. (2010) Isotopic evidence for Fe cycling and repartitioning in ancient oxygen-deficient settings: examples from black shales of the mid-to-late Devonian Appalachian basin. *Earth Planet. Sci. Lett.* **290**, 244–253.

- Fehr M. A., Anderson P. S., Halenius U. and Mörth C.-M. (2008) Iron isotope variations in Holocene sediments of the Gotland Deep, Baltic Sea. *Geochim. Cosmochim. Acta* **72**, 807–826.
- Fehr M. A., Anderson P. S., Halenius U. and Mörth C.-M. (2010) Iron enrichments and Fe isotopic composition of surface sediments from the Gotland Deep, Baltic Sea. *Chem. Geol.* **277**, 310–322.
- Fossing H. and Jørgensen B. B. (1989) Measurement of bacterial sulfate reduction in sediments: evaluation of a single-step chromium reduction method. *Biogeochemistry* **8**, 205–222.
- Frost C. D., von Blanckenburg F., Schoenberg R., Frost B. R. and Swapp S. M. (2007) Preservation of Fe isotope heterogeneities during diagenesis and metamorphism of banded iron formation. *Contrib. Mineral. Petrol.* **153**, 211–235.
- Glangeaud P. (1916) Le cratère-lac Pavin et le volcan de Monchalm (Puy-de-Dôme). *C. R. Acad. Sci.* **162**, 428–430.
- Guilbaud R., Butler I. B., Ellam R. M. and Rickard D. (2010) Fe isotope exchange between Fe(II)_{aq} and nanoparticulate mackinawite (FeS_m) during nanoparticulate growth. *Earth Planet. Sci. Lett.* **300**, 174–183.
- Guilbaud R., Butler I. B. and Ellam R. M. (2011) Abiotic pyrite formation produces a large Fe isotope fractionation. *Science* **332**, 1548–1551.
- Habicht K. S., Gade M., Thamdrup B., Berg P. and Canfield D. E. (2002) Calibration of sulfate levels in the Archean Ocean. *Science* **298**, 2372–2374.
- Halverson G. P., Poitrasson F., Hoffman P. F., Nédélec A., Montel J.-M. and Kirby J. (2011) Fe isotope and trace element geochemistry of the Neoproterozoic syn-glacial Rapitan iron formation. *Earth Planet. Sci. Lett.* **309**, 100–112.
- Heimann A., Johnson C. M., Beard B. L., Valley J. W., Roden E. E., Spicuzza M. J. and Beukes N. J. (2010) Fe, C, and O isotope compositions of banded iron formation carbonates demonstrate a major role for dissimilatory iron reduction in ~2.5 Ga marine environments. *Earth Planet. Sci. Lett.* **294**, 8–18.
- Holland H. D. (1984) *The Chemical Evolution of the Atmosphere and Oceans*. Princeton Series in Geochemistry. Princeton University Press, Princeton, NJ, 598 pp.
- Hongve D. (1997) Cycling of iron, manganese, and phosphate in a Meromictic Lake. *Limnol. Oceanogr.* **42**, 635–647.
- Huerta-Diaz M. A. and Morse J. W. (1990) A quantitative method for determination of trace metal concentrations in sedimentary pyrite. *Mar. Chem.* **29**, 119–144.
- Icopini G. A., Anbar A. D., Ruebush S. S., Tien M. and Brantley S. L. (2004) Iron isotope fractionation during microbial reduction of iron: the importance of adsorption. *Geology* **32**, 205–208.
- Jarzecki A. A., Anbar A. D. and Spiro T. G. (2004) DFT analysis of Fe(H₂O)₆³⁺ and Fe(H₂O)₆²⁺ structure and vibrations: implications for isotope fractionation. *J. Phys. Chem. A* **108**, 2726–2732.
- Jézéquel D., Sarazin G., Prévot F., Viollier E., Groleau A., Agrinier P., Albéric P., Binet S., Bergonzini L. and Michard G. (2011) Bilan hydrique du lac Pavin – water balance of the Lake Pavin. *Rev. Sci. Nat. d'Auvergne* **74**, 75–96.
- Johnson C. M., Skulan J. L., Beard B. L., Sun H., Neilson K. H. and Braterman P. S. (2002) Isotopic fractionation between Fe(III) and Fe(II) in aqueous solutions. *Earth Planet. Sci. Lett.* **195**, 141–153.
- Johnson C. M., Beard B. L., Beukes N. J., Klein C. and O'Leary J. M. (2003) Ancient geochemical cycling in the Earth as inferred from Fe isotope studies of banded iron formations from the Transvaal Craton. *Contrib. Mineral. Petrol.* **144**, 523–547.
- Johnson C. M., Beard B. L., Klein C., Beukes N. J. and Roden E. E. (2008a) Iron isotopes constrain biologic and abiologic processes in banded iron formation genesis. *Geochim. Cosmochim. Acta* **72**, 151–169.
- Johnson C. M., Beard B. L. and Roden E. E. (2008b) The iron isotope fingerprints of redox and biogeochemical cycling in modern and ancient Earth. *Annu. Rev. Earth Planet. Sci.* **36**, 457–493.
- Juvigné E. and Gilot E. (1986) Age et zones de dispersion de téphra émises par les volcans du Montcineyre et du lac Pavin (Massif Central, France). *Z. Dtsch. Geol. Ges.* **137**, 613–623.
- Kappler A., Pasquero C., Konhauser K. O. and Newman D. K. (2005) Deposition of banded iron formations by anoxygenic phototrophic Fe(II)-oxidizing bacteria. *Geology* **33**, 865–868.
- Konhauser K. O., Lalonde S. V., Amskold L. and Holland H. D. (2007) Was there really an Archean phosphate crisis? *Science* **315**, 1234.
- Konhauser K. O., Lalonde S. V., Planavsky N. J., Pecoits E., Lyons T. W., Mojzsis S. J., Rouxel O. J., Barley M. E., Rosiere C., Fralick P. W., Kump L. R. and Bekker A. (2011) Aerobic bacterial pyrite oxidation and acid rock drainage during the Great Oxidation Event. *Nature* **478**, 369–373.
- Lehours A.-C., Evans P., Bardot C., Joblin K. and Fonty G. (2007) Phylogenetic diversity of Archea and bacteria in the anoxic zone of a meromictic lake (Lake Pavin, France). *Appl. Environ. Microb.* **73**, 2016–2019.
- Lehours A.-C., Batisson I., Guedon A., Mailhot G. and Fonty G. (2009) Diversity of culturable bacteria, from the anaerobic zone of the meromictic Lake Pavin, able to perform dissimilatory-iron reduction in different in vitro conditions. *Geomicrobiol. J.* **26**, 212–223.
- Lopes F., Viollier E., Thiam A., Michard G., Abril G., Groleau A., Prévot F., Carrias J.-F. and Jézéquel D. (2011) Biogeochemical modeling of anaerobic vs. aerobic methane oxidation in a meromictic crater lake (Lake Pavin, France). *Appl. Geochem.* **26**, 1919–1932.
- Lyons T. W. and Severmann S. (2006) A critical look at iron paleoredox proxies: new insights from modern euxinic marine basins. *Geochim. Cosmochim. Acta* **70**, 5698–5722.
- Malinovsky D. N., Stenberg A., Rodushkin I., Andren H., Ingri J., Ohlander B. and Baxter D. C. (2003) Performance of high resolution MC-ICP-MS for Fe isotope ratio measurements in sedimentary geological materials. *J. Anal. At. Spectrom.* **18**, 687–695.
- Malinovsky D. N., Rodyushkin I. V., Scherbakova E. P., Ponter C., Ohlander B. and Ingri J. (2005) Fractionation of Fe isotopes as a result of redox processes in a basin. *Geochem. Int.* **43**, 797–803.
- Martin J.-M. (1985) The Pavin Crater Lake. In: W. Stumm (Editor), *Chemical processes in lakes. Reviews in Mineralogy and Geochemistry*. John Wiley & Sons, New York, pp. 169–188.
- Matthews A., Morgans-Bell H. S., Emmanuel S., Jenkyns H. C., Erel Y. and Halicz L. (2004) Controls on iron-isotope fractionation in organic-rich sediments (Kimmeridge Clay, Upper Jurassic, southern England). *Geochim. Cosmochim. Acta* **68**, 3107–3123.
- Meybeck M., Martin J. M. and Olive P. (1975) Géochimie des eaux et des sédiments de quelques lacs volcaniques du Massif Central français. *Verh. Internat. Verein. Limnol.* **19**, 1150–1164.
- Michard G., Viollier E., Jézéquel D. and Sarazin G. (1994) Geochemical study of a crater lake: Lac Pavin, France – identification, location and quantification of the chemical reactions in the lake. *Chem. Geol.* **115**, 103–115.
- Michard G., Jézéquel D. and Viollier E. (2003) Vitesses des réactions de dissolution et précipitation au voisinage de l'interface oxydo-réducteur dans un lac méromictique: Le lac Pavin (Puy-de-Dôme, France). *Revue des Sciences de l'Eau* **16**, 199–218.
- Olive P. and Boulègue J. (2004) Biogeochemical study of a meromictic lake: Pavin lake, France. *Geomorphologie* **4**, 305–316.

- Planavsky N., Rouxel O., Bekker A., Shapiro R., Fralick P. and Knudsen A. (2009) Iron-oxidizing microbial ecosystems thrived in late Paleoproterozoic redox-stratified oceans. *Earth Planet. Sci. Lett.* **286**, 230–242.
- Planavsky N., McGoldrick P., Scott C. T., Li C., Reinhard C. T., Kelly A. E., Chu X., Bekker A., Love G. D. and Lyons T. W. (2011) Widespread iron-rich conditions in the mid-Proterozoic ocean. *Nature* **477**, 448–451.
- Planavsky N., Rouxel O., Bekker A., Hofmann A., Little C. T. S. and Lyons T. (2012) Iron isotope composition of some Archean and Proterozoic iron formations. *Geochim. Cosmochim. Acta* **180**, 158–169.
- Polyakov V. B., Clayton R. N., Horita J. and Mineev S. D. (2007) Equilibrium iron isotope fractionation factors of minerals: reevaluation from the data of nuclear inelastic resonant X-ray scattering and Mössbauer spectroscopy. *Geochim. Cosmochim. Acta* **71**, 3833–3846.
- Poulton S. W. and Canfield D. E. (2011) Ferruginous conditions: a dominant feature of the ocean through Earth's history. *Elements* **7**, 107–112.
- Rouxel O. J., Dobbek N., Ludden J. and Fouquet Y. (2003) Iron isotope fractionation during oceanic crust alteration. *Chem. Geol.* **202**, 155–182.
- Rouxel O. J., Bekker A. and Edwards K. J. (2005) Iron isotope constraints on the Archean and Paleoproterozoic ocean redox state. *Science* **307**, 1088–1091.
- Schettler G., Schwab M. J. and Stebich M. (2007) A 700 years record of climate change based on geochemical and palynological data from varved sediments (Lac Pavin, France). *Chem. Geol.* **240**, 11–35.
- Schirmermeister B. E., de Vos J. M., Antonelli A. and Bagheri H. C. (2013) Evolution of multicellularity coincided with increased diversification of cyanobacteria and the Great Oxidation Event. *Proc. Natl. Acad. Sci. USA* **110**, 1791–1796.
- Schoenberg R. and von Blanckenburg F. (2005) An assessment of the accuracy of stable Fe isotope ratio measurements on samples with organic and inorganic matrices by high-resolution multicollector ICP-MS. *Int. J. Mass Spectrom.* **242**, 257–275.
- Severmann S., Johnson C. M., Beard B. L. and McManus J. (2006) The effect of early diagenesis on the Fe isotope compositions of porewaters and authigenic minerals in continental margin sediments. *Geochim. Cosmochim. Acta* **70**, 2006–2022.
- Severmann S., Lyons T. W., Anbar A. D., McManus J. and Gordon G. (2008) Modern iron isotope perspective on the benthic iron shuttle and the redox evolution of ancient oceans. *Geology* **36**, 487–490.
- Skulan J. L., Beard B. L. and Johnson C. M. (2002) Kinetic and equilibrium Fe isotope fractionation between aqueous Fe(III) and hematite. *Geochim. Cosmochim. Acta* **66**, 2995–3015.
- Song L., Liu C.-Q., Wang Z.-L., Zhu X., Teng Y., Liang L., Tang S. and Li J. (2011) Iron isotope fractionation during biogeochemical cycle: information from suspended particulate matter (SPM) in Aha Lake and its tributaries, Ghizhou, China. *Chem. Geol.* **280**, 170–179.
- Staubwasser M., von Blanckenburg F. and Schoenberg R. (2006) Iron isotopes in the early marine diagenetic iron cycle. *Geology* **34**, 629–632.
- Staubwasser M., Schoenberg R., von Blanckenburg F., Krüger S. and Pohl C. (2013) Isotope fractionation between dissolved and suspended particulate Fe in the oxic and anoxic water column of the Baltic Sea. *Biogeosciences* **10**, 233–245.
- Steinboefel G., Horn I. and von Blanckenburg F. (2009) Microscale tracing of Fe and Si isotope signatures in banded iron formation using femtosecond laser ablation. *Geochim. Cosmochim. Acta* **73**, 5343–5360.
- Steinboefel G., von Blanckenburg F., Horn I., Konhauser K. O., Beukes N. J. and Gutzmer J. (2010) Deciphering formation processes of banded iron formations from the Transvaal and the Hamersley successions by combined Si and Fe isotope analysis using UV femtosecond laser ablation. *Geochim. Cosmochim. Acta* **74**, 2677–2696.
- Strelow F. W. E. (1980) Improved separation of iron from copper and other elements by anion-exchange chromatography on a 4% cross-linked resin with high concentrations of hydrochloric acid. *Talanta* **27**, 727–732.
- Sumner D. Y. (1997) Carbonate precipitation and oxygen stratification in late Archean seawater as deduced from facies and stratigraphy of the Gamohaian and Frisco formations, Transvaal Supergroup, South Africa. *Am. J. Sci.* **297**, 455–487.
- Takayanagi K. and Cossa D. (1997) Vertical distribution of Sb(III) and Sb(V) in Pavin Lake, France. *Water Res.* **31**, 671–674.
- Taylor S. R. and McLennan S. M. (1985) *The continental crust: its composition and evolution*. Blackwell Scientific Publications, Oxford, 312 p.
- Taylor P. D. P., Maeck R. and De Bievre P. (1992) Determination of the absolute isotopic composition and atomic weight of a reference sample of natural iron. *Int. J. Mass Spectrom.* **121**, 111–125.
- Teutsch N., Schmid M., Müller B., Halliday A. N., Bürgmann H. and Wehrli B. (2009) Large iron isotope fractionation at the oxic-anoxic boundary in Lake Nyos. *Earth Planet. Sci. Lett.* **285**, 52–60.
- Tsikos H., Matthews A., Erel Y. and Moore J. M. (2010) Iron isotopes constrain biogeochemical redox cycling of iron and manganese in a Paleoproterozoic stratified basin. *Earth Planet. Sci. Lett.* **298**, 125–134.
- Valaas Hyslop E., Valley J. W., Johnson C. M. and Beard B. L. (2008) The effects of metamorphism on O and Fe isotope compositions in the Biwabik Iron Formation, northern Minnesota. *Contrib. Mineral. Petrol.* **155**, 313–328.
- Viollier E., Jézéquel D., Michard G., Pèpe M., Sarazin G. and Albéric P. (1995) Geochemical study of a crater lake (Pavin Lake, France): trace-element behaviour in the monimolimnion. *Chem. Geol.* **125**, 61–72.
- Viollier E., Michard G., Jézéquel D., Pèpe M. and Sarazin G. (1997) Geochemical study of a crater lake: Lake Pavin, Puy de Dôme, France. Constraints afforded by the particulate matter distribution in the element cycling within the lake. *Chem. Geol.* **142**, 225–241.
- Viollier E., Inglett P. W., Hunter K., Roychoudhury A. N. and Van Cappellen P. (2000) The ferrozine method revisited: Fe(II)/Fe(III) determination in natural waters. *Appl. Geochem.* **15**, 785–790.
- Viollier E., Thiam A., Darmoul Y., Neubert N., Nägler T., Lopes F., Michard G., Jézéquel D. (2014) Molybdenum isotopes fractionation in a crater lake: understanding the signature of biogeochemical processes interplay. Submitted.
- Virtasalo J., Whitehouse M. J. and Kotilainen A. T. (2013) Iron isotope heterogeneity in pyrite fillings of Holocene worm burrows. *Geology* **41**, 39–42.
- von Blanckenburg F., Mamberti M., Schoenberg R., Kamber B. S. and Webb G. E. (2008) The iron isotope composition of microbial carbonate. *Chem. Geol.* **249**, 113–128.
- Wang M., Jiang Y. Y., Kim K. M., Qu G., Ji H. F., Mittenthal J. E., Zhang H. Y. and Caetano-Anollés G. (2011) A universal molecular clock of protein folds and its power in tracing the early history of aerobic metabolism and planet oxygenation. *Mol. Biol. Evol.* **28**, 567–582.
- Welch S. A., Beard B. L., Johnson C. M. and Braterman P. S. (2003) Kinetic and equilibrium Fe isotope fractionation

- between aqueous Fe(II) and Fe(III). *Geochim. Cosmochim. Acta* **67**, 4231–4250.
- Weyer S. and Schwieters J. B. (2003) High precision Fe isotope measurements with high mass resolution MC-ICPMS. *Int. J. Mass Spectrom.* **226**, 355–368.
- Wu L., Druschel G., Findlay A., Beard B. L. and Johnson C. M. (2012) Experimental determination of iron isotope fractionations among $\text{Fe}_{\text{aq}}^{2+}$ - FeS_{aq} -Mackinawite at low temperatures: implications for the rock record. *Geochim. Cosmochim. Acta* **89**, 46–61.
- Yamaguchi K. E., Johnson C. M., Beard B. L. and Ohmoto H. (2005) Biogeochemical cycling of iron in the Archean-Paleoproterozoic Earth: constraints from iron isotope variations in sedimentary rocks from the Kaapvaal and Pilbara Cratons. *Chem. Geol.* **218**, 135–169.
- Yoshiya K., Nishizawa M., Sawaki Y., Ueno Y., Komiya T., Yamada K., Yoshida N., Hirata T., Wada H. and Maruyama S. (2012) In situ iron isotope analyses of pyrite and organic carbon isotope ratios in the Fortescue Group: metabolic variations of a Late Archean ecosystem. *Precamb. Res.* **212**, 169–193.

Associate editor: Nicolas Dauphas

APPENDIX A. Procedure for the analysis of accurate Fe isotope composition

Iron separation by ion chromatography

Before isotopic analysis, Fe must be separated from other elements contained in the sample matrix that can affect the mass bias in the mass spectrometer and/or form complex compounds creating interference on Fe masses. Major isobaric interferences may derive from (i) neighbor elements such as Cr^+ and Ni^+ on the masses 54 and 58 respectively, or (ii) sample matrix elements such as Ca that lead to molecular interferences such as $^{40}\text{Ca}^{16}\text{O}^+$ and $^{40}\text{Ca}^{17}\text{O}^+$ interfering on the masses 56 and 57, respectively. Doubly charged species such as Pd^{2+} , Cd^{2+} , Sn^{2+} can also induce interferences at masses 54, 56 and 57. The most commonly used method to separate Fe from other elements is based on anion exchange chromatography in HCl medium (Strelow, 1980). Over the last decade, several laboratories have developed similar techniques for Fe separation by chromatography (Beard and Johnson, 1999; Malinovsky et al., 2003; Rouxel et al., 2003; Poitrasson et al., 2004; Dauphas et al., 2004; Schoenberg and von Blanckenburg, 2005). We follow essentially the chemical protocol laid out by Dauphas et al. (2004).

Sample chemistry was implemented in a clean laboratory at the Laboratory of Geochemistry and Cosmochemistry, IPGP. Water samples were loaded in Teflon beakers and evaporated to dryness. They were twice acidified with mixtures of HCl-HNO₃ and evaporated, to ensure that all Fe is in the ferric state before loading on the resin. Bulk sediment and volcanic rock samples analyzed over the course of this study were digested in a sequence of acid mixtures including HF, HCl and HNO₃. All samples were finally dissolved in 6 M HCl before ion exchange chromatography. The following ion chromatography procedure was performed twice for each sample to ensure separation of Fe from matrix

elements. Bio-Rad Poly-Prep columns were filled with 1 mL anion exchange resin (AG1-X8 200-400mesh chloride form). The resin was cleaned three times with 10 ml H₂O and 5 ml 1 M HNO₃. It was then preconditioned in HCl medium by running 10 ml H₂O, 10 ml 0.4 M HCl, 5 ml H₂O and 2 ml 6 M HCl. Half of the sample solution (250 µl) was loaded on the column in 6 M HCl (containing between 10 and 500 µg of Fe). Matrix elements were eluted with 8 ml 6 M HCl, whereas Fe(III) is strongly adsorbed on the resin and is quantitatively retained. Fe was subsequently eluted in 10 ml 0.4 M HCl, with a procedural yield of >94%. The Fe blank level of the present procedure has been evaluated by systematic analyses of one blank in each sample series, prepared as described above but without any sample powder or solution. The blank was always below 40 ng Fe (average ~30 ng), thus representing less than 0.4 % of the bulk Fe.

Mass spectrometry

Iron concentrations and isotopic compositions were measured using a Neptune ThermoFischer MC-ICP-MS (Multiple Collector Inductively Coupled Plasma Mass Spectrometer) at the Laboratory of Geochemistry and Cosmochemistry. The Neptune is equipped with eight adjustable Faraday cups and one fixed center cup. Iron isotopes were measured simultaneously at masses 54, 56, 57 and 58, while the contributions of Cr and Ni on masses 54 and 58 were monitored and corrected for by using ion intensities measured at masses 53 and 60, respectively. Masses 53, 54, 56, 57, 58 and 60 were collected in the Faraday cups Low 3, Low 2, C, High 1, High 2 and High 4, respectively. A drawback in the use of the MC-ICP-MS is that polyatomic argide interferences are produced from Ar plasma (Weyer and Schwieters, 2003; Anbar, 2004; Dauphas and Rouxel, 2006; Dauphas et al., 2009). These are mainly ⁴⁰Ar¹⁴N⁺, ⁴⁰Ar¹⁶O⁺, ⁴⁰Ar¹⁶OH⁺ and ⁴⁰Ar¹⁸O⁺ interfering at m/z 54, 56, 57 and

58, respectively. Iron isotopes were fully resolved from argide interferences using the high-resolution mode of the Neptune (for details see Weyer and Schwieters, 2003). This high-resolution mode allows us to achieve a resolving power with $m/\Delta m$ of $\sim 12,500$. Sample solutions were nebulized and introduced using two different systems: the ThermoFinnigan stable introduction system (SIS) and the ESI Apex-HF desolvating apparatus. We found that the signal intensity was more stable with the SIS system but the Apex-HF apparatus gave better sensitivity (~ 3 times more signal) and better precision on the Fe isotope measurement, in agreement with previous results from another study (Schoenberg and von Blanckenburg, 2005). Thus all measurements presented herein were carried out with the Apex-HF apparatus.

The samples were analyzed in 0.3 M HNO_3 at a concentration of ~ 0.6 ppm Fe. Nebuliser uptake rate was between 40 to 60 $\mu\text{l}/\text{min}$. Signal intensity on the mass 56 was between 10 to 15 volts with the high-mass resolution mode. Fe isotope measurements were performed only when a flat Fe shoulder-peak plateau with a width > 200 ppm was achieved. The analytical routine included baseline correction measured for 120 s before each acquisition. Each sample measurement consisted of 1 block of 20 cycles with 7.2 seconds duration. The take up time before analysis and wash time after analysis were fixed at 70 and 120 seconds respectively.

Instrumental mass discrimination was corrected for using the conventional sample-standard bracketing (SSB) approach (Belshaw et al., 2000; Beard et al., 2003; Rouxel et al., 2003; Albarède and Beard, 2004). The SSB method was shown to give results as accurate and precise as the Cu-dopping method for correction of instrumental mass bias during Fe isotope measurement (Schoenberg and von Blanckenburg, 2005; Dauphas et al., 2009). The $^{56}\text{Fe}/^{54}\text{Fe}$ and $^{57}\text{Fe}/^{54}\text{Fe}$ ratios were expressed in the usual δ notation in per mil (‰) as,

$$\delta^{56}\text{Fe} = \left[\left(\frac{^{56}\text{Fe}}{^{54}\text{Fe}} \right)_{\text{sample}} / \left(\frac{^{56}\text{Fe}}{^{54}\text{Fe}} \right)_{\text{standard}} - 1 \right] \times 1000$$

$$\delta^{57}\text{Fe} = \left[\left(\frac{{}^{57}\text{Fe}}{{}^{54}\text{Fe}} \right)_{\text{sample}} / \left(\frac{{}^{57}\text{Fe}}{{}^{54}\text{Fe}} \right)_{\text{standard}} - 1 \right] \times 1000$$

where the standard is IRMM-014, a pure synthetic Fe metal from the Institute for Reference Materials and Measurements (Taylor et al., 1992). A comparison between two solutions of IRMM-014 prepared respectively in IPG Paris and at the Origins Laboratory of the University of Chicago showed homogeneous Fe isotopic composition, with $\delta^{56}\text{Fe}$ of $0.021 \pm 0.032 \text{ ‰}$ and $\delta^{57}\text{Fe}$ of $-0.017 \pm 0.064 \text{ ‰}$ (2σ ; $n = 27$).

Accuracy and analytical precision

Three water samples collected in Lac Pavin were selected to test if they could be affected by any matrix effect during column chemistry and/or Fe isotope measurement. In order to gauge matrix effects, we replaced Fe contained in the water samples with Fe that has a known isotope composition. After preparation of the selected samples in 6 M HCl medium as described in the experimental section, they were passed through a first column. The matrix was recovered (6 M HCl fraction) and passed through a second column to get rid of any potential residual Fe. The Fe-free matrix was doped with 50 μg of IRMM-014 (*i.e.* our Fe standard from the Institute for Reference Materials and Measurements). These solutions of Fe-free matrix+IRMM-014 were processed twice through column chemistry and analyzed on the Neptune as described above. The results are presented in Table A.1. The three solutions of Fe-free matrix+IRMM-014 show Fe isotope compositions undistinguishable, within error, from pure IRMM-014 standard (*i.e.* $\delta^{56}\text{Fe} \sim 0\text{‰}$). Iron quantification by MC-ICP-MS also indicates that the final solution contained $> 47 \mu\text{g}$ Fe thus yielding more than 94% of the bulk Fe initially introduced. These data illustrate that the present procedure is not affected by any matrix effect and that the yield is near 100 %.

We assessed the accuracy and analytical precision through the analysis of multiple preparations of individual geostandards. Such replicate analyses take into account not only the external precision of the technique, but various parameters such as the nature of the sample and variations due to chemical separation and handling. Because no standards have been characterized for Fe isotope composition of lakes or river waters, we analyzed international rock geostandards (Dauphas and Rouxel, 2006; Craddock and Dauphas, 2010). Specifically, we used the geostandards (i) IF-G: a 3.8 Ga old BIF (Banded Iron Formation) from Isua (Greenland), (ii) BCR-2: a basalt from Columbia River (Portland, Oregon), (iii) AC-E: a granite from Ailsa Craig Island (SW Scotland). These 3 geostandards represent various lithologies, thus allowing us to test further if any matrix effect may occur. Interestingly they cover a large range of Fe contents from high (39.10 wt%) to low (1.77 wt%) concentration, providing an opportunity to test the sensitivity of the technique. Iron isotope compositions of IF-G, BCR-2 and AC-E geostandards measured over five years in our laboratory are shown in Figure A.1 and their weighted averages are given in Table A.1. Mean $\delta^{56}\text{Fe}$ values of IF-G (102 analyses of 23 solutions), BCR-2 (59 analyses of 10 solutions) and AC-E (29 analyses of 5 solutions) were 0.637 ± 0.049 , 0.082 ± 0.060 , and 0.337 ± 0.048 ‰ respectively (2SD, *i.e.* Standard Deviation), in good agreement with available data for these geostandards (*e.g.* 0.647 ± 0.025 ‰, 0.091 ± 0.025 ‰ and 0.322 ± 0.025 ‰ in Dauphas et al., 2009; see also Fe standards compilation in Dauphas and Rouxel, 2006; Craddock and Dauphas, 2010). These results demonstrate the accuracy of our measurements. The long-term reproducibility on the mass spectrometer was also evaluated from the analyses of a pure Fe solution that was measured regularly over a 5-years period. This "in house" solution, named ALD, is a solution from ALDRICH (catalog number 35,630-1), which was diluted to 0.6 ppm in 0.3 M HNO_3 , in order to match IRMM-014 Fe concentration. Thirty-six measurements of ALD gave $\delta^{56}\text{Fe}$ and $\delta^{57}\text{Fe}$ values of 0.373 ± 0.054 and 0.546 ± 0.120 ‰ (2SD), respectively (Fig. A.1). The

reproducibility on $\delta^{56}\text{Fe}$ and $\delta^{57}\text{Fe}$ for ALD is similar to the reproducibility obtained on several solutions of IF-G, BCR-2 and AC-E, which represent different Fe chemical separates after chromatography. This indicates that the chemistry does not introduce any variability in the Fe isotope composition. The accuracy seems to be as good as the reproducibility, *i.e.* better than 0.06 ‰ for $\delta^{56}\text{Fe}$ and 0.12 ‰ for $\delta^{57}\text{Fe}$ (2SD). The larger uncertainty observed on the $^{57}\text{Fe}/^{54}\text{Fe}$ ratio relative to the $^{56}\text{Fe}/^{54}\text{Fe}$ ratio is likely a consequence of the greater difference in the isotope abundances. A three-isotope plot for the standards together with all Lac Pavin samples (n=141) analyzed in the course of this study is presented in Figure A.2. All data points plot on a single mass fractionation line, with a slope of 1.480 and an intercept value (0.005) not significantly different from 0. This again illustrates the reliability of our Fe isotope measurements.

Collection of anoxic water samples for Fe isotope analyses

The collection of water samples is devoted to the analysis of either dissolved species or particulate matter. The separation of dissolved species from particles is usually performed through a filtration process where the particles are retained on a filter. When anoxic water samples are filtered under atmospheric conditions, we must make sure that redox sensitive elements initially dissolved in water do not precipitate on the filter. For instance, Fe can be highly concentrated as dissolved Fe(II) in anoxic water. When samples are taken up to the surface, they can be contaminated by atmospheric oxygen and Fe(III) precipitate may form. Partial precipitation of Fe(III)-oxyhydroxyde from dissolved Fe(II) leads to a strong isotope fractionation up to $\sim 3\%$ in $^{56}\text{Fe}/^{54}\text{Fe}$ ratio (Johnson et al., 2002; Welch et al., 2003; Jarzecki et al., 2004; Anbar et al., 2005). In the present work, Fe-rich water samples from the anoxic zone (75 m depth) of Lac Pavin have been collected in November 2006 using a lab-made 50

ml PE syringe sampler (Viollier et al., 1995) and filtered directly *in situ* (0.2 μm Millipore filter with Luer connexion) from the syringe. Two kinds of filtration were performed either (i) at depth during water collection (*i.e.* during introduction of water into the syringe) or (ii) under atmospheric condition just after taken up the syringe to the surface (Table A.2). Both methods lead to identical Fe concentrations and isotope compositions for the dissolved Fe (samples LP2006-7 and LP2006-8 were filtered at depth, while samples LP2006-5 and LP2006-6 were filtered in surface just after retrieving the sampler). Accordingly, filtration at the surface does not modify Fe concentrations or isotope compositions when sampling anoxic waters.

REFERENCES

- Albarède F. and Beard B.L. (2004) Analytical methods for non-traditional isotopes. In: C.M. Johnson, B.L. Beard and F. Albarède (Editors), *Geochemistry of non-traditional stable isotopes*. Mineralogical Society of America and Geochemical Society, Washington DC., pp. 113-152.
- Anbar A.D. (2004) Iron stable isotopes: beyond biosignatures. *Earth Planet. Sci. Lett.* **217**, 223-236.
- Anbar A.D., Jarzecki A.A. and Spiro T.G. (2005) Theoretical investigation of iron isotope fractionation between $\text{Fe}(\text{H}_2\text{O})_6^{3+}$ and $\text{Fe}(\text{H}_2\text{O})_6^{2+}$: Implications for iron stable isotope geochemistry. *Geochim. Cosmochim. Acta* **69**, 825-837.
- Beard B.L. and Johnson C.M. (1999) High precision iron isotope measurements of terrestrial and lunar materials. *Geochim. Cosmochim. Acta* **63**, 1653-1660.
- Beard B.L., Johnson C.M., Skulan J.L., Neilson K.H., Cox L. and Sun H. (2003) Application of Fe isotopes to tracing the geochemical and biological cycling of Fe. *Chem. Geol.* **195**, 87-117.
- Belshaw N.S., Zhu X.K. and O'Nions R.K. (2000) High precision measurement of iron isotopes by plasma source mass spectrometry. *Int. J. Mass Spectrom.* **197**, 191-195.
- Craddock P. and Dauphas N. (2010) Iron isotopic compositions of geological reference material and chondrites. *Geostandards and Geoanalytical Research* **35**, 101-123.
- Dauphas N., Janney P.E., Mendybaev R.A., Wadhwa M., Richter F., Davis A.M., van Zuilen M., Hines R. and Foley C.N. (2004) Chromatographic separation and multicollection-ICPMS analysis of iron - Investigating mass-dependent and -independent isotope effects. *Anal. Chem.* **76**, 5855-5863.
- Dauphas N., Pourmand A. and Teng F.-Z. (2009) Routine isotopic analysis of iron by HR-MC-ICPMS: How precise and how accurate? *Chem. Geol.* **267**, 175-184.
- Dauphas N. and Rouxel O.J. (2006) Mass spectrometry and natural variations of iron isotopes. *Mass. Spectrom. Rev.* **25**, 515-550.

- Jarzecki A.A., Anbar A.D. and Spiro T.G. (2004) DFT analysis of $\text{Fe}(\text{H}_2\text{O})_6^{3+}$ and $\text{Fe}(\text{H}_2\text{O})_6^{2+}$ structure and vibrations: implications for isotope fractionation. *J. Phys. Chem. A*. **108**, 2726-2732.
- Johnson C.M., Skulan J.L., Beard B.L., Sun H., Nealon K.H. and Braterman P.S. (2002) Isotopic fractionation between Fe(III) and Fe(II) in aqueous solutions. *Earth Planet. Sci. Lett.* **195**, 141-153.
- Malinovsky D.N., Stenberg A., Rodushkin I., Andren H., Ingri J., Ohlander B. and Baxter D.C. (2003) Performance of high resolution MC-ICP-MS for Fe isotope ratio measurements in sedimentary geological materials. *J. Anal. At. Spectrom.* **18**, 687-695.
- Poitrasson F., Halliday A.N., Lee D.-C., Levasseur S. and Teutsch N. (2004) Iron isotope differences between Earth, Moon, Mars and Vesta as possible records of contrasted accretion mechanisms. *Earth Planet. Sci. Lett.* **223**, 253-266.
- Rouxel O., Dobbek N., Ludden J. and Fouquet Y. (2003) Iron isotope fractionation during oceanic crust alteration. *Chem. Geol.* **202**, 155-182.
- Schoenberg R. and von Blanckenburg F. (2005) An assessment of the accuracy of stable Fe isotope ratio measurements on samples with organic and inorganic matrices by high-resolution multicollector ICP-MS. *Int. J. Mass Spectrom.* **242**, 257-275.
- Strelow F.W.E. (1980) Improved separation of iron from copper and other elements by anion-exchange chromatography on a 4% cross-linked resin with high concentrations of hydrochloric acid. *Talanta* **27**, 727-732.
- Taylor P.D.P., Maeck R. and De Bièvre P. (1992) Determination of the absolute isotopic composition and atomic weight of a reference sample of natural iron. *Int. J. Mass Spectrom.* **121**, 111-125.
- Viollier E., Jézéquel D., Michard G., Pèpe M., Sarazin G. and Albéric P. (1995) Geochemical study of a crater lake (Pavin Lake, France): Trace-element behaviour in the monimolimnion. *Chem. Geol.* **125**, 61-72.
- Welch S.A., Beard B.L., Johnson C.M. and Braterman P.S. (2003) Kinetic and equilibrium Fe isotope fractionation between aqueous Fe(II) and Fe(III). *Geochim. Cosmochim. Acta* **67**, 4231-4250.
- Weyer S. and Schwieters J.B. (2003) High precision Fe isotope measurements with high mass resolution MC-ICPMS. *Int. J. Mass Spectrom.* **226**, 355-368.

Table A.1

Average Fe isotope composition of geostandards and analytical tests performed on water samples.

Type	Sample	Description	Fe (wt%)	$\delta^{56}\text{Fe}$ (‰)	$\delta^{57}\text{Fe}$ (‰)
Banded Iron Formation	IF-G	SARM Geostandard	39.10	0.637 ± 0.049 (n=102)	0.943 ± 0.100 (n=102)
Basalt	BCR-2	USGS Geostandard	9.66	0.082 ± 0.060 (n=59)	0.125 ± 0.098 (n=59)
Granite	AC-E	USGS Geostandard	1.77	0.337 ± 0.048 (n=29)	0.487 ± 0.122 (n=29)
"Home" standard	ALD	Aldrich Fe solution	-	0.373 ± 0.054 (n=36)	0.546 ± 0.120 (n=36)
Reference	IRMM/LP2006-1D	IRMM-014 in LP2006-1 matrix	-	0.043 ± 0.060	0.062 ± 0.132
Reference	IRMM/LP2006-2D	IRMM-014 in LP2006-2 matrix	-	0.004 ± 0.052	0.031 ± 0.102
Reference	IRMM/LP2006-3D	IRMM-014 in LP2006-3 matrix	-	0.032 ± 0.070	0.054 ± 0.086

Uncertainties correspond to 2SD (standard deviation).

IF-G: distributed by the SARM (Service d'Analyse des Roches et des Minéraux) of the CRPG (Centre de Recherche Pétrographique et Géochemie) in Nancy, France

BCR-2 and AC-E: distributed by the USGS (United States Geological Survey).

ALD: pure Fe solution (ALDRICH: catalog No 35,630-1; 9833mg/ml of Fe in 5% HNO₃).

Table A.2

Depth, Fe concentration and Fe isotope composition of water samples from Lac Pavin, collected in November 2006.

Sample	Filtration type	Depth (m)	Fe (μM)	$\delta^{56}\text{Fe}$ (‰)	$\delta^{57}\text{Fe}$ (‰)
LP2006-1	atmospheric conditions	61.5	77	-0.80 ± 0.08	-1.20 ± 0.14
LP2006-2	atmospheric conditions	62	153	-0.64 ± 0.04	-0.95 ± 0.06
LP2006-2-duplicate	atmospheric conditions	62	160	-0.71 ± 0.08	-1.00 ± 0.16
LP2006-3	atmospheric conditions	62.5	264	-0.46 ± 0.06	-0.70 ± 0.10
LP2006-4	atmospheric conditions	70	727	0.00 ± 0.02	0.05 ± 0.08
LP2006-5	atmospheric conditions	75	874	0.06 ± 0.04	0.12 ± 0.12
LP2006-6	atmospheric conditions	75	855	0.07 ± 0.04	0.10 ± 0.08
LP2006-7	At depth (75m)	75	841	0.06 ± 0.06	0.08 ± 0.06
LP2006-8	At depth (75m)	75	853	0.05 ± 0.04	0.06 ± 0.10

Uncertainties correspond to 2SD (standard deviation).

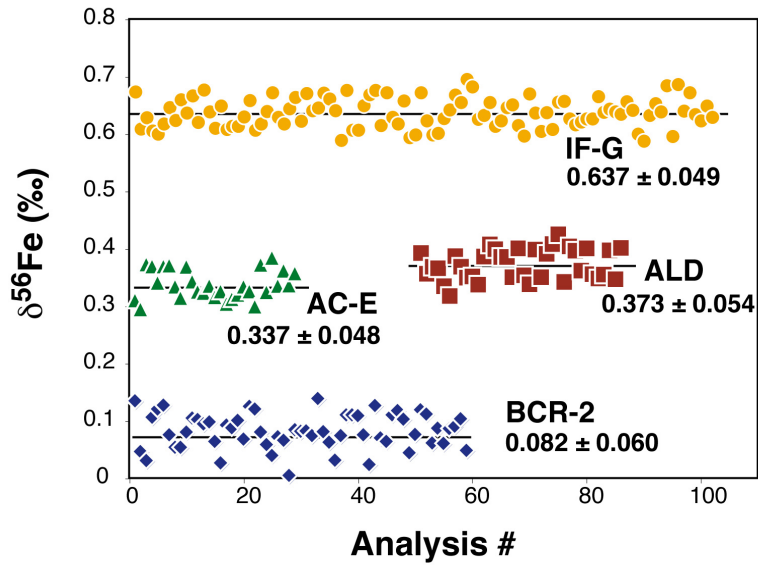


Fig. A.1. Iron isotope composition of international (IF-G, AC-E, BCR-2) and "home" (ALD) standards. Analyzes over a 5-years period. Mean $\delta^{56}\text{Fe}$ values are reported with 2SD uncertainty and are in excellent agreement with previous data for these standards.

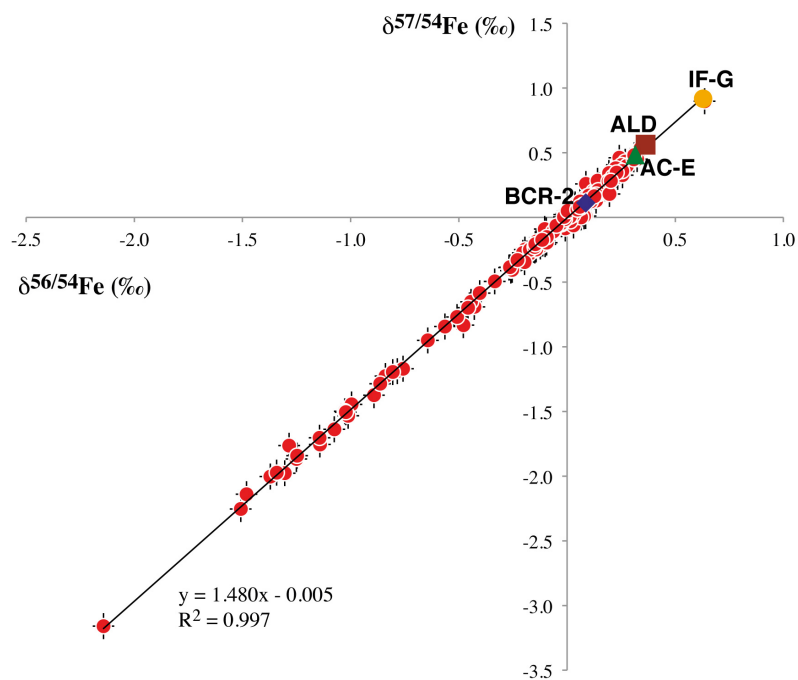


Fig. A.2. Three-isotope plot representing $\delta^{57}\text{Fe}$ versus $\delta^{56}\text{Fe}$. Data measured for international (IF-G, AC-E, BCR-2) and "home" (ALD) standards, together with Lac Pavin samples analyzed in the course of this study ($n=141$). All data plot on a single mass fractionation line, with a slope close to the theoretical value (~ 1.5).